nature portfolio

Peer Review File

High energy resolution CsPbBr3 alpha particle detector with a full-customized readout application specific integrated circuit

Reviewers' comments:

Reviewer #1 (Remarks to the Author):

The article titled "Unprecedented energy resolution of perovskite CsPbBr3 single-crystal detector for alpha particle detection" presents a significant advancement in the field of radiation detection. The authors describe the development of a CsPbBr3 single-crystal detector that demonstrates an exceptionally high energy resolution for alpha particles. By optimizing the crystal's growth process to reduce defects and implementing a Schottky electrode, they achieved lower dark current and enhanced high-temperature stability. The introduction of a customized readout ASIC further improved the detector's performance, achieving a record energy resolution of 1.1% for 5.5 MeV alpha particles from Americium-241 without additional signal processing. These improvements make the CsPbBr3 detector a promising candidate for applications requiring precise radiation detection and measurement, offering advantages over traditional semiconductor detectors in terms of operation temperature range, energy resolution, and stability.
However, the manuscript, while presenting an intriguing study, is noted to lack detailed descriptions of experiments, such as:
• The thinning experiment is inadequately described. It lacks information on the initial thickness of the crystal, the extent of thinning, and any subsequent surface treatments.
• The description of the optimized custom electronic scheme is insufficient, rendering it difficult for others in the field to replicate this methodology based on the provided information.
Minor comments include:
• The title is perceived as somewhat unscientific. A more descriptive title, such as "High Energy Resolution…" would be preferable, reflecting the achieved results.
• In Figure 1, it would be more effective to display the scale of Epair on the top Y axis, rather than using color coding.

Reviewer #2 (Remarks to the Author):

This study introduces a CsPbBr3 detector aimed at α-particle detection, achieving energy resolution of 1.1% through crystal thinning, and the integration of a custom ASIC. However, the manuscript suffers from a critical absence of experimental details, leaving numerous procedures and conditions unexplained across the main text and supplementary materials, thus undermining its reference value and reproducibility. Comparisons drawn may be unreliable, notably with referenced CdZnTe devices that seemingly do not share the same device structure with the CsPbBr3 detector. This study’s breakthrough and innovation are insufficient, especially considering that Y.H. et al., in 2021, achieved a comparable energy resolution of 1.4% for the more challenging γ detection using the same CsPbBr3 material. The mechanism to get better device performance through crystal thinning is also unclear. Given these considerations, I would not recommend this manuscript for publication in Nature Communications.

1. “an ideal α detection set-up should be sensitive and stable,” indicating that sensitivity is a positive attribute. However, it later describes, “Unfortunately, the state-of-the-art CdZnTe detector is sensitive to high doses of radiation,” suggesting sensitivity is a disadvantage. This inconsistent use of the term ‘sensitive’ could confuse readers.

2. The authors don't present the full name "inverse temperature crystallization" for "ITC" before its first use. Additionally, the atomic percentages of the elements listed in Table S1 don't correspond to CsPbBr3, CsPb2Br5, or a mixture. The proportions appear unreasonable, and the authors should explain this discrepancy.

3. The authors highlight the first use of thinning and polishing to improve the leakage current issues in CsPbBr3 crystal devices. Fig. 2b reflects successful enhancements in crystal quality and reduced leakage currents through these processes. For the sake of scientific rigor and reproducibility, it is necessary to provide specific methods of thinning and polishing. However, the manuscript does not provide any details such as the tools used, the parameters of the process, and whether thinning was performed across all faces of the crystal.

4. The thinning of the crystal aims to remove surface CsPb2Br5 defects to reduce leakage current. The authors have already shown SEM images depicting surface defects before thinning. A comparison of SEM results before and after thinning would straightforwardly and persuasively demonstrate the changes in surface defects. The authors have not included such a comparative analysis. Additionally, presenting any significant and justifiable variations in the EDS results pre- and post-thinning could decisively confirm the effectiveness of this method.

5. The resistivity measurement shown in Fig. S2 is reported at a voltage range (-0.1 to 0.1 V) that is significantly lower than the device's tolerance and operational voltages(>100 V). The authors should consider extending the voltage range to better align with the actual conditions in which the detector will be used.

6. "Fig. 2d presents the variation of element atomic percentage as a function of etching time based on the XPS spectra of each element, which indicates that the Sn diffusion into CsPbBr3 is lower than that of other electrodes38." It is scientifically inaccurate to compare the variation of atomic percentage with etching time to literature values without considering the potential differences in etch rates. The authors should present the atomic percentage variation concerning the actual etching depth, which would allow for a more accurate comparison with the Sn electrode thickness and a clearer indication of the extent of Sn diffusion. Furthermore, when comparing electrode oxidation, the stability of the In/LiF electrode configuration cited (Fig. 5c) appears to be on par with the Sn electrodes used in this study. Therefore, the assertion of superior stability for the Sn/CsPbBr3 interface lacks compelling evidence.

7. The authors have successfully suppressed the device leakage current under reverse bias using a Schottky-type structure, as evidenced by the significant difference in current under forward and reverse biases shown in Fig. 2c and Fig. 2f. It would be important to clarify whether the CdZnTe based device used for comparison in leakage current experiments also employed a Schottky-type structure. As seen in Fig. S9, the CdZnTe detector employs an Au/CdZnTe/Au. Without this information, the comparison may not be fair.

8. "the detector is much thick" should be "the detector is much thicker".
"the contribution of electrons to charge can be ignored when the radiation source is incident from the anode electrode (Fig. S7)," The direct line depicted in Fig. S7 suggests a simplistic model. It would be beneficial for the authors to elaborate on the methodology or formulae used to derive this relationship, as various factors such as interface defects, crystal imperfections, and the actual behavior of charge carriers in the presence of an electric field

could significantly influence this contribution.

9. The authors have conducted numerous tests in vacuum conditions without specifying the operational details on how the vacuum was achieved. The difference in mobility values obtained in air and vacuum (42 $cm^2 \cdot V^{-1} \cdot s^{-1}$ and 49 $cm^2 \cdot V^{-1} \cdot s^{-1}$, respectively) is not substantial. Are these values measured from the same device in different environments or from separate devices tested in each condition?

10. The authors have characterized the high-temperature stability of the device by analyzing the rise time distribution at various temperatures (Fig. 3e). However, the rise time distribution at room temperature already exhibits considerable variability, which raises questions about the intrinsic stability of the device or the consistency of the α-source.
Given the known issues with perovskite response drift and instability during long-term storage, especially when using Sn electrodes prone to oxidation, it is imperative that the authors conduct further tests focused on the robustness and stability of the detector over prolonged periods.

11. Could the authors clarify whether the 1.1% energy resolution was achieved under vacuum conditions?

12. Y. H. et al. achieved an energy resolution of 1.4% for γ-particle detection using the same CsPbBr3 material in 2021 (Nat. Photon., 15, 36-42(2021)), comparable to the energy resolution for α-particle detection in this work. Given the typically more complex interaction pathways and broader energy spectrum of γ-particles, achieving finer energy resolution is more challenging for γ detection than for α detection. Therefore, the breakthrough significance of this work appears limited

Reviewer #3 (Remarks to the Author):

This work by Zhang et al demonstrated an alpha particle detector with high energy resolution below 1.1%. By thinning the CsPbBr3 crystal, they improved the crystal quality by removing the unwanted phase and extended defects, and thus a low dark current. They have characterized the carrier mobility, trap density of the thinned crystal to validate this point. Finally, they have investigated the alpha-particle detection performance with their device in great details. While the demonstrated performance is highly promising, the main concern is the poor material innovation of this work which does not warrant the publication in a high profile journal like Nature Comm. Simply thinning the crystal yields very little control over the final product. If the crystal defects are located all through the bulk, this method would not be applicable anymore. In other words, the main finding or method of this work is not broadly applicable to other perovskite crystal system. Its potential impact could be very limited. I hesitate to recommend its publication in Nature Comm in its current format.

The detailed technical comments are listed below:
- The improvement by the thinning method is not well understood. It is not clear why CsPb2br5 would be the unwanted phase. If it's an insulator phase, it should not contribute to the dark current. It is also not clear what type of extended defects are there at the surface, and why could thinning remove them without causing other types of surface defects?

- From the current discussion, it is not clear why Sn/perovskite interface is stable as SnO peaks were observed at the interface. Literature studies cited by the author also suggested

that Sn can diffuse into the perovskite structure causing instability. And what is special in this case that makes the interface stable?

- The extremely slow rise time of the CspbBr3 detector is not understood in Fig. 4a-b. There is a long tail near the slower side (100 us) which persist at higher bias (40 us). How is the rise time compared to other perovskite crystals, and what's the impact of crystal thinning on the rise time? And why would higher temperatures narrow the rise time distribution?

- The operational stability (under irradiation and under electrical field stress) should be measured.

Response to Referees

Reviewer #1 (Remarks to the Author):

The article titled "Unprecedented energy resolution of perovskite $CsPbBr_3$ single-crystal detector for alpha particle detection" presents a significant advancement in the field of radiation detection. The authors describe the development of a $CsPbBr_3$ single-crystal detector that demonstrates an exceptionally high energy resolution for alpha particles. By optimizing the crystal's growth process to reduce defects and implementing a Schottky electrode, they achieved lower dark current and enhanced high-temperature stability. The introduction of a customized readout ASIC further improved the detector's performance, achieving a record energy resolution of 1.1% for 5.5 MeV alpha particles from Americium-241 without additional signal processing. These improvements make the $CsPbBr_3$ detector a promising candidate for applications requiring precise radiation detection and measurement, offering advantages over traditional semiconductor detectors in terms of operation temperature range, energy resolution, and stability.

However, the manuscript, while presenting an intriguing study, is noted to lack detailed descriptions of experiments, such as:

1. The thinning experiment is inadequately described. It lacks information on the initial thickness of the crystal, the extent of thinning, and any subsequent surface treatments.

Response: We thank the reviewer for appreciating the significant of our paper. We simplified description of the thinning experiment in previous manuscript due to the word limit., In the revised manuscript, we have discussed the thinning experiments in the Methods.

Changes in manuscript: "The as-grown $CsPbBr_3$ crystals with thicknesses of ~1.5 mm were firstly grilled to ~1.2 mm by using 2000, 3000, 5000, and 7000 mesh sandpaper, successively. Then, the crystals were mechanically polished to ~1.1 mm with MgO powders (size of ~3 μm) in ethanol. Finally, the samples were finely polished to ~1 mm by nano-sized MgO (30 nm) with surface roughness of 2.77 nm (Fig. S21). Note that all six sides of the crystal need to be polished. Subsequently, the polished $CsPbBr_3$ crystals were rinsed in cyclohexane and blew dried with nitrogen gas to remove surface impurities."

Changes in SI: Fig. R1 is added as Supplementary Fig. 21.

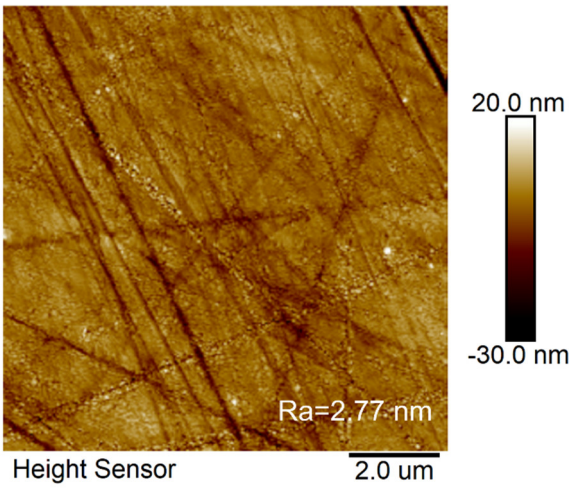

Fig. R1 AFM images of wafer surface after surface process.

2. The description of the optimized custom electronic scheme is insufficient, rendering it difficult for others in the field to replicate this methodology based on the provided information.

Response: Thank the Reviewer's suggestion. In the revised manuscript, a detailed discussion of the optimized custom electronic scheme is added. The main additions are as follows:

(1) A discussion and explanation of each part of the readout circuit has been added;

(2) The design of readout circuit which fit to the relatively low mobility $CsPbBr_3$ is added.

Changes in manuscript: "As shown in Fig. 5a and Fig. S18, one channel of the ASIC is mainly composed of a charge sensitive amplifier (CSA) and a CR-$(RC)^4$ slow shaper, which is beneficial to improve the signal-to-noise ratio and obtain a semi-gaussian wave. The CSA is adopted to amplify and convert the charges induced by particles into voltage, whose gain is determined by its feedback capacitance. In fact, the slow shaper is a band-pass filter to decrease the noise. Thus, the output amplitude of the shaper is directly proportional to the energy of the particles."

"The output of the 2^{nd} stage is connected to the chip pad to measure the higher-energy particles since each stage of the shaper provides a separate gain. Moreover, the output of the 4^{th} stage is utilized for low-noise applications."

"The proposed ASIC was fabricated and evaluated using standard commercial CMOS processing. As shown in Fig. 5b, the amplitude of the slow shaper output voltage is monotonically increasing as the input charge increases, which tends to be saturated when the peaking time becomes larger. Thus, to decrease the die area, the resistors of the slow shaper are realized by the transistors that operate in the linear region, of which the on-resistance varies with a lower gate-source voltage. Additionally, both a maximum charge-voltage conversion gain and a minimum equivalent noise charge (ENC) of the proposed ASIC are achieved at a peaking time of ~2.5 μs (Figs. 5c and 5d)."

Minor comments include:

3. The title is perceived as somewhat unscientific. A more descriptive title, such as "High Energy Resolution…" would be preferable, reflecting the achieved results.

Response: Thank the Reviewer's suggestion. The title has changed to "*High energy resolution perovskite $CsPbBr_3$ single-crystal detector for alpha particle detection*".

4. In Figure 1, it would be more effective to display the scale of Epair on the top Y axis, rather than using color coding.

Response: Thank the Reviewer's suggestion. In the revised manuscript, the Figure 1 has been modified to display the scale of *E*pair on the top Y axis.

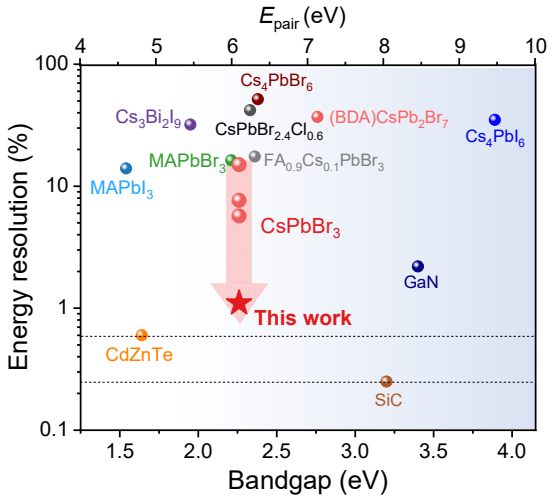

Fig. R2 Evolution of compound semiconductors performance.

Reviewer #2 (Remarks to the Author):

This study introduces a $CsPbBr_3$ detector aimed at α-particle detection, achieving energy resolution of 1.1% through crystal thinning, and the integration of a custom ASIC. However, the manuscript suffers from a critical absence of experimental details, leaving numerous procedures and conditions unexplained across the main text and supplementary materials, thus undermining its reference value and reproducibility. Comparisons drawn may be unreliable, notably with referenced CdZnTe devices that seemingly do not share the same device structure with the $CsPbBr_3$ detector. This study's breakthrough and innovation are insufficient, especially considering that Y.H. et al., in 2021, achieved a comparable energy resolution of 1.4% for the more challenging γ detection using the same $CsPbBr_3$ material. The mechanism to get better device performance through crystal thinning is also unclear. Given these considerations, I would not recommend this manuscript for publication in Nature Communications.

Response: We thank the reviewer's insightful comments and feedback. We have carefully modified the manuscript with comprehensive explanations in the revised version.

(1) The thinning method, device stability and ASIC are been supplemented in both main text and supporting information.

(2) Both Au/CdZnTe/Au and Au/$CsPbBr_3$/Sn are Schottky-type devices. The CdZnTe detector is a double-Schottky and the $CsPbBr_3$ detector is a single Schottky, both of which operate in the same voltage-mode. Therefore, the comparison is appropriate.

(3) The difference between high-energy particle detection and gamma-ray detection is explained in the following specific comment. Based on our results and the work reported by Y.H. et al., we believe the $CsPbBr_3$ detectors have broad application in radiation detection fields.

(4) The mechanism to achieve better device performance through crystal thinning is more plentifully explained in the revised manuscript.

1. "an ideal α detection set-up should be sensitive and stable," indicating that sensitivity is a positive attribute. However, it later describes, "Unfortunately, the state-of-the-art CdZnTe detector is sensitive to high doses of radiation," suggesting sensitivity is a disadvantage. This inconsistent use of the term 'sensitive' could confuse readers.

Response: Thank for the Reviewer pointing this out. In the revised manuscript, the relative discussion has been improved.

Changes in manuscript: "Unfortunately, the state-of-the-art CdZnTe detectors are tend to be severely damaged under high irradiation doses[28] and not able to operate at high temperatures due to the relatively narrow band gap (1.64 eV @ RT)."

2. The authors don't present the full name "inverse temperature crystallization" for "ITC" before its first use. Additionally, the atomic percentages of the elements listed in Table S1

don't correspond to $CsPbBr_3$, $CsPb_2Br_5$, or a mixture. The proportions appear unreasonable, and the authors should explain this discrepancy.

Response: Thank the reviewer's comments. We have added the full name "inverse temperature crystallization" for "ITC" in the revised manuscript.

To further confirm the proportions of $CsPb_2Br_5$ second phase (SP) defects, batches of $CsPbBr_3$ crystals are characterized by both the SEM and EDS. The well-defined $CsPb_2Br_5$ particles with regular polyhedral morphologies in $CsPbBr_3$ crystal were identified. Typical SP defects with different shapes were evaluated and compared with the $CsPbBr_3$ matrix, as shown in Fig. R3 (a)-(d). Since the small size of the $CsPb_2Br_5$ phases (usually less than 10 μm) and the limited accuracy in composition testing of EDS, the atomic ratio tends to be slightly fluctuated[1, 2]. The composition at points 1, 3 and 5, that locate at the SP, exhibit an atomic ratio close to Cs: Pb: Br≈1: 2: 5, which determines the $CsPb_2Br_5$ phase. The points 2, 4 and 6 from the $CsPbBr_3$ matrix show a ratio of 1: 1: 3 for Cs: Pb: Br. The corresponding EDS results are listed in Table R1.

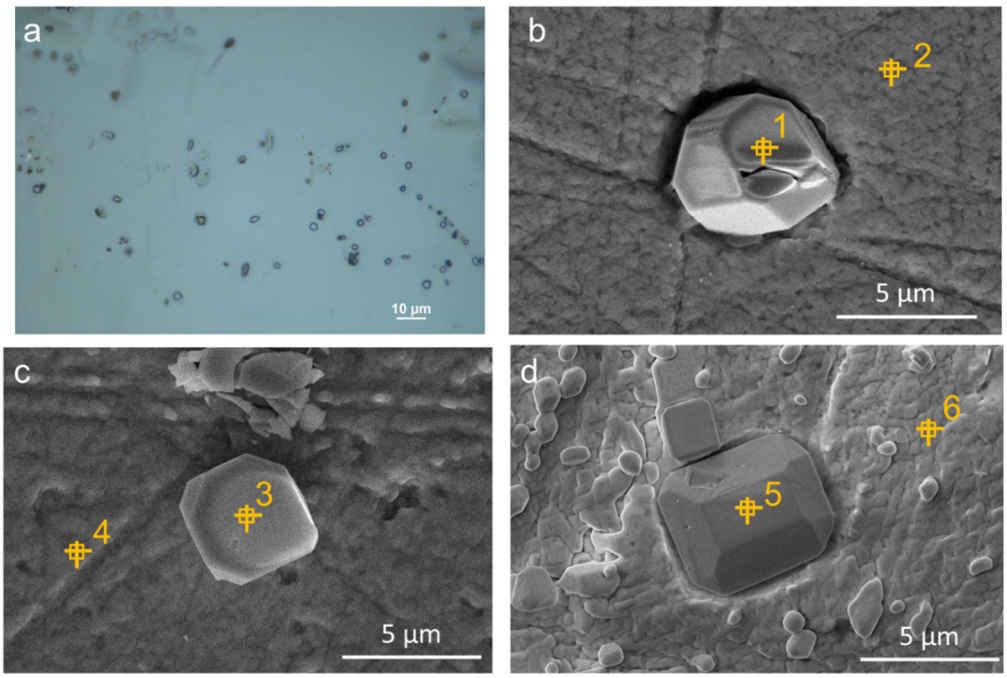

Fig. R3 (a) The optical microscope image (b)-(d) Typical SEM images of $CsPb_2Br_5$ phases particles with regular polyhedral morphology.

Table R1 The atomic percentage of the elements at different sites measured by EDS micro-area test.

Elements	1	2	3	4	5	6
Cs	12.23 %	21.25 %	13.10 %	20.18 %	12.48 %	20.12%
Pb	25.97 %	19.12 %	24.62 %	19.99 %	26.69 %	19.78 %
Br	61.79 %	59.62 %	62.28 %	59.83 %	60.33 %	60.10 %
Total	100 %	100 %	100 %	100 %	100 %	100 %

Changes in SI: Fig. R3 is optimized as Supplementary Fig. 1, Tabel R1 is added as Supplementary Table 1.

3. The authors highlight the first use of thinning and polishing to improve the leakage current issues in $CsPbBr_3$ crystal devices. Fig. 2b reflects successful enhancements in crystal quality and reduced leakage currents through these processes. For the sake of scientific rigor and reproducibility, it is necessary to provide specific methods of thinning and polishing. However, the manuscript does not provide any details such as the tools used, the parameters of the process, and whether thinning was performed across all faces of the crystal.
Response: We simplified description of the thinning experiment in previous manuscript due to the word limit., In the revised manuscript, we have discussed the thinning experiments in the Methods.

Changes in the manuscript: "The as-grown $CsPbBr_3$ crystals with thicknesses of ~1.5 mm were firstly grilled to ~1.2 mm by using 2000, 3000, 5000, and 7000 mesh sandpaper, successively. Then, the crystals were mechanically polished to ~1.1 mm with MgO powders (size of ~3 μm) in ethanol. Finally, the samples were finely polished to ~1 mm by nano-sized MgO (30 nm) with surface roughness of 2.77 nm (Fig. S21). Note that all six sides of the crystal need to be polished. Subsequently, the polished $CsPbBr_3$ crystals were rinsed in cyclohexane and blew dried with nitrogen gas to remove surface impurities."

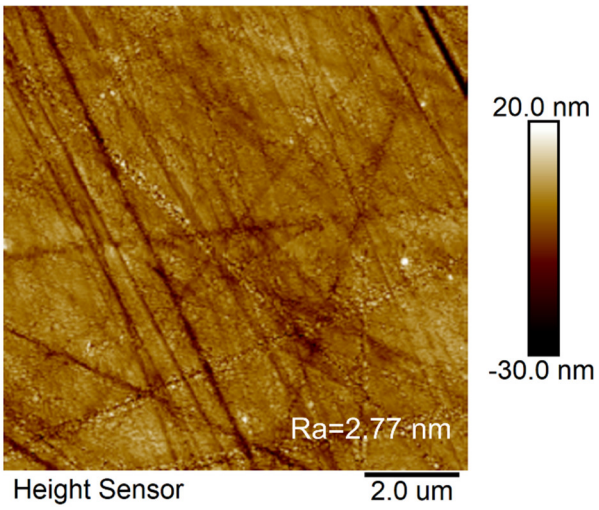

Fig. R4 AFM images of wafer surface after surface process

Changes in SI: Fig. R4 is added as Supplementary Fig. 21.

4. The thinning of the crystal aims to remove surface $CsPb_2Br_5$ defects to reduce leakage current. The authors have already shown SEM images depicting surface defects before thinning. A comparison of SEM results before and after thinning would straightforwardly and persuasively demonstrate the changes in surface defects. The authors have not included such a comparative analysis. Additionally, presenting any significant and justifiable variations in the EDS results pre- and post-thinning could decisively confirm the effectiveness of this method.

Response: Thanks for the reviewer's suggestion. To further compare the SEM results before and after thinning, we selected three typical of $CsPbBr_3$ grown by the ITC method. The $CsPbBr_3$ crystal was thinned to different thicknesses with intervals of 0.1 mm to observe the distribution and size of the $CsPb_2Br_5$ phase defects along the growth direction (perpendicular to the main face) of the crystal, as shown in Fig. R5. As the thinning progresses, the proportion of the secondary phase gradually decreases (Table R2). For example, the proportion of $CsPb_2Br_5$ phase defect decreases from 24.8% to 11.4% further to 5.1%, which indicating that the thinning method effectively eliminate the defect-rich region in the near-surface region of $CsPbBr_3$ crystals.

Additionally, EDS measurements indicate that the SP exhibit an atomic ratio close to Cs: Pb: Br≈1: 2: 5, and the matrix show a ratio close to Cs: Pb: Br≈1: 1: 3. At the same time, the proportion of SP decreases gradually with thinning.

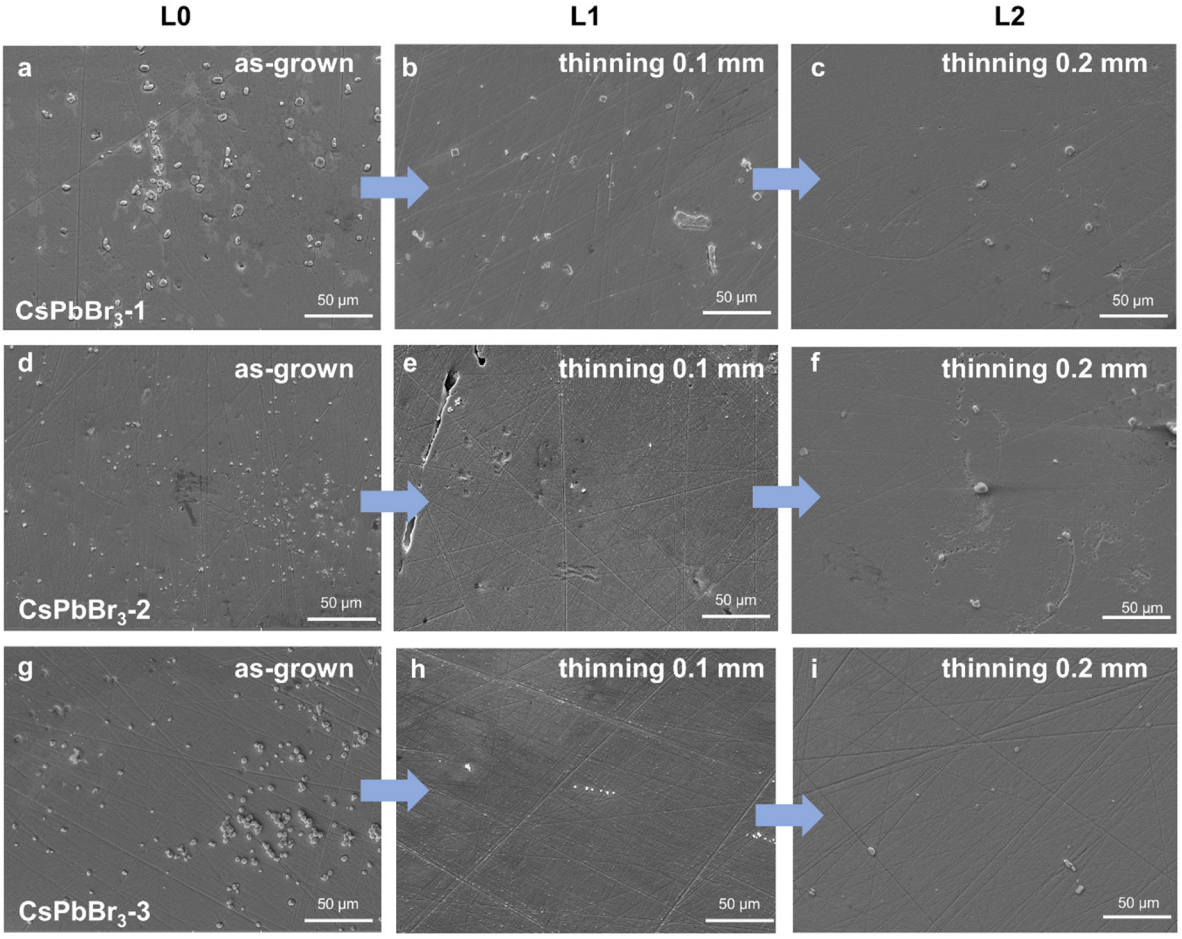

Fig. R5 The typical SEM images of spatial inhomogeneous distribution of the $CsPbBr_3$ surface along the vertical thickness of the $CsPbBr_3$ crystal. (a) $CsPbBr_3$-1 before and (b) (c) after thinning. (d) $CsPbBr_3$-2 before and (e) (f) after thinning. (g) $CsPbBr_3$-3 before and (h) (i) after thinning.

Table R2 The proportion of SP before and after thinning

	L0	L1	L2
$CsPbBr_3$-1	24.8%	11.4%	5.1%
$CsPbBr_3$-2	7.5%	3.9%	1.7%
$CsPbBr_3$-3	9.2%	4.2%	1.1%

Changes in manuscript: "To further compare the SEM results before and after thinning, batches of as-grown $CsPbBr_3$ single crystals were evaluated (Fig. S2 and Table S2). The $CsPb_2Br_5$ defects gradually decrease as thinning, indicating that the higher concentration of $CsPb_2Br_5$ tends to be distributed near the $CsPbBr_3$ surface."

Changes in SI: Fig. R5 is added as Supplementary Fig. 2 and Table R2 is added as Supplementary Table 2.

5. The resistivity measurement shown in Fig. S2 is reported at a voltage range (-0.1 to 0.1 V) that is significantly lower than the device's tolerance and operational voltages (>100 V). The authors should consider extending the voltage range to better align with the actual conditions in which the detector will be used.

Response: Thank the Reviewer's comments. According to the reference[3], the bulk leakage current at high bias is mainly limited by the barrier height between the electrode and the crystals (Fig. R6). However, there is no significant contribution of the contact barrier on the measured bulk resistance in the low-bias. Therefore, it is more accurate to measure bulk resistivity at low-bias.

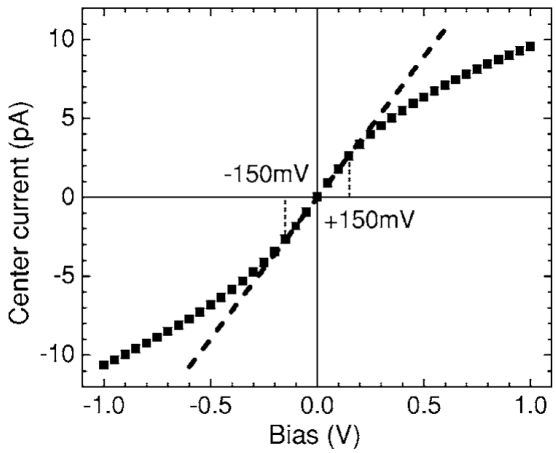

Fig. R6 Current-voltage characteristics measured on single crystal detector and linear fit in the bulk resistivity limited range[3].

First, for semi-insulating $CsPbBr_3$ crystals, Au electrodes are usually deposited by evaporation to form the test devices. The difference between the metal work function and the electron affinity of the $CsPbBr_3$ crystal inevitably leads to the formation of a barrier at the

metal $CsPbBr_3$ interface. The Ohmic behavior can generally obtained when the bias voltage is small enough, which means that the barrier between $CsPbBr_3$ and Au is negligible[3]. Second, at room temperature, the on-state current increases linearly with the applied voltage and the resistance value remains constant in the lower voltage range. At high voltages, the movement of ions increases, leading to more rapid increases in current compared to the applied voltage, while causing a decrease in material resistance. Consequently, the higher the applied test voltage, the lower the resistance of the material, resulting in a potentially large difference in resistance measurements when materials at different voltages. Therefore, resistance tests are usually performed at relatively lower voltages, as shown in Fig. R7 (a).

The dark current density of the Au/$CsPbBr_3$/Au detector at high voltage (200 V) is still not satisfied for detection over a long period of time, as shown in Fig. R7 (b). For this reason, a Schottky-type Sn/$CsPbBr_3$/Au detector was fabricated, and their current values under actual use conditions are shown in Figs. 2d and 2h.

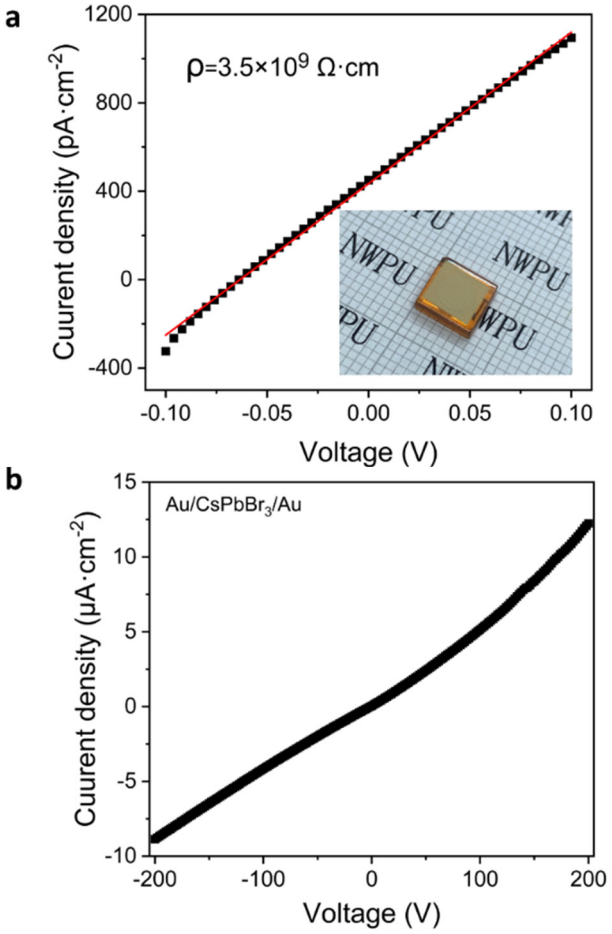

Fig. R7 The typical *I-V* curves of the Au/$CsPbBr_3$/Au device ranging from (a) -0.1 V to 0.1 V and (b) -200 V to 200 V.

Changes in manuscript: "However, the dark current density of the $CsPbBr_3$ devices with the symmetric electrodes is still not satisfied for long-term operational, even after thinning (Fig. S3)."

Changes in SI: Fig. R7 is added as Supplementary Fig. 3.

6. “Fig. 2d presents the variation of element atomic percentage as a function of etching time based on the XPS spectra of each element, which indicates that the Sn diffusion into $CsPbBr_3$ is lower than that of other electrodes[38].” It is scientifically inaccurate to compare the variation of atomic percentage with etching time to literature values without considering the potential differences in etch rates. **(a)** The authors should present the atomic percentage variation concerning the actual etching depth, which would allow for a more accurate comparison with the Sn electrode thickness and a clearer indication of the extent of Sn diffusion. **(b)** Furthermore, when comparing electrode oxidation, the stability of the In/LiF electrode configuration cited (Fig. 5c) appears to be on par with the Sn electrodes used in this study. Therefore, the assertion of superior stability for the Sn/$CsPbBr_3$ interface lacks compelling evidence.

Response: Thank the Reviewer’s question. The question can be divided into two parts.

Question (a): To determine the etch rate, we employ a combined approach of Atomic Force Microscopy (AFM) and X-ray Photoelectron Spectroscopy (XPS).

First, the thickness of the Sn electrode was determined using AFM. To avoid the diffusion thickness caused by the reaction between the electrode and the crystal, the Sn electrode was fabricated on a Si wafer by the evaporation method. At the same time, to minimize the error caused by XPS etching, the thickness of the Sn electrode was slightly thicker than the test thickness, about 191 nm, as shown in Fig. R8.

Then the Sn electrode was etched with XPS (4 keV, Ar^+), and the corresponding etching time was recorded. As shown in Fig. R9, the peak of Si appeared after 11 minutes, indicating that the Sn electrode was completely etched away. Therefore, the etch rate of XPS for the Sn electrode is calculated with a value of approximately 17.36 nm/min. However, the etching rate is the rate of the elemental Sn. There are three regions in Sn/$CsPbBr_3$ etching, include Sn electrode, the diffusion region of Sn with $CsPbBr_3$, and the $CsPbBr_3$ single crystal. It should also be noted that the etching rates are dependent on the target, which means that the eating rate is different in the above areas. Therefore, we refer to other literature using the etching time as the X axis[4].

To further determine the extent of the reaction, an analysis of the chemical state of Pb at the interface was conducted[4, 5], as shown in Fig. R10. The ratio of the peak areas of Pb^0 and Pb^{2+} was fitted to quantify the extent of the reaction between metal and $CsPbBr_3$[5]. The corresponding redox equations are presented as follows:

$$Pb^{2+} + 2e^- = Pb^0$$

The Pb^0/Pb^{2+} ratio of Sn and $CsPbBr_3$ devices is 0.14. Compared with the reference[5] (*ACS Appl. Mater. Interfaces*, **15**, 51370-51379, 2023), this ratio is the same as that of the optimized Au/Al/BCP/C_{60}/$CsPbBr_3$/Au structure, which is used to suppress ion migration and interface electrochemical reactions.

Thus, there is a stable contact with negligible reaction between Sn and $CsPbBr_3$.

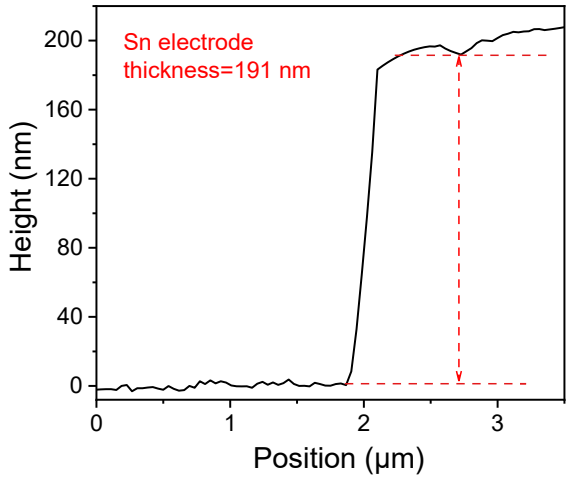

Fig. R8 The thickness of Sn electrode measured by AFM

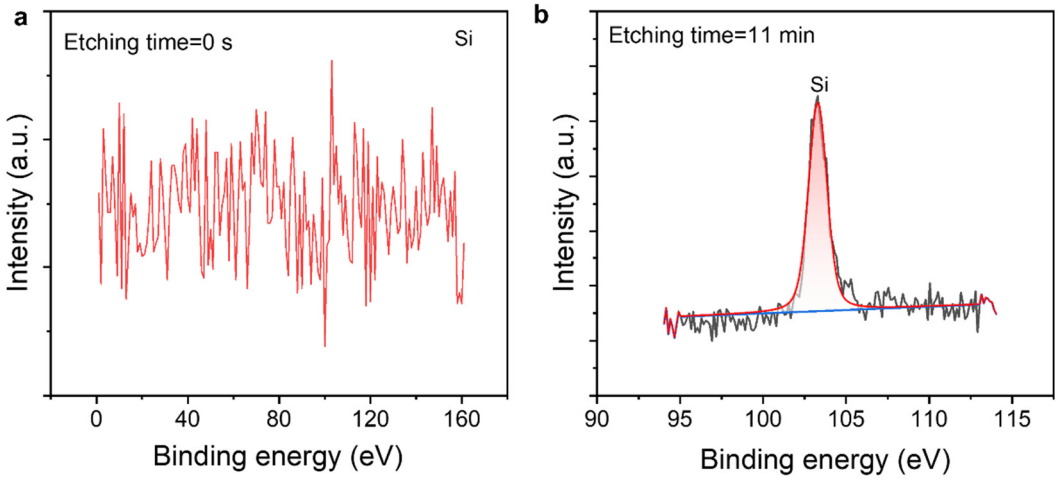

Fig. R9 X-ray photoelectron spectroscopy (XPS) measurements of Si element with different eating time. (a) 0 s. (b) 11 min.

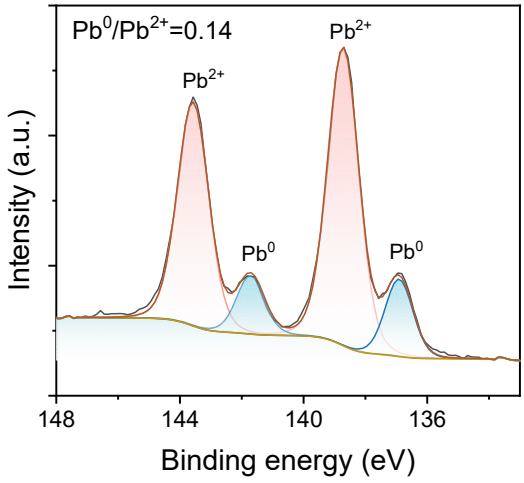

Fig. R10 The XPS results of Pb elements of Sn and $CsPbBr_3$.

Changes in manuscript: Fig. R10 is added as Fig. 2g

"In addition, the chemical state of Sn at the interface was determined, which showed a weak Sn-Br peak at 486.74 eV (Fig. 2f), indicating an inevitable reaction[38, 40]. To quantify the reaction, the peak area ratio of Pb^0 and Pb^{2+} is fitted according to the corresponding redox equation[39, 42, 43]:

$$Pb^{2+} + 2e^- = Pb^0 \quad (2)$$

The Pb^0/Pb^{2+} ratio is 0.14 for Sn/$CsPbBr_3$/Au (Fig. 2g), that is comparable to the optimized Au/Al/BCP/C_{60}/$CsPbBr_3$/Au structure[42], which demonstrate a stable contact with negligible reaction between Sn and $CsPbBr_3$."

Question (b): In the cited reference[6], the LiF interlayer is employed in the $CsPbBr_3$ Schottky junction radiation detector to prevent atomic reaction between the crystal and metal electrode (In). As mentioned by the reviewer, the interface stability of the Sn electrode is comparable to that of LiF interlayer insertion, and the preparation process is simpler. In addition, although the reaction diffusion between the crystal and the electrode can be reduced by optimizing the thickness of the intermediate layer and the preparation process, the existence of the interface will have an impact on the carrier transport and charge collection efficiency. Therefore, it is concluded that the interfacial stability of Sn is relatively stable based on the results of XPS and device stability experiments.

7. The authors have successfully suppressed the device leakage current under reverse bias using a Schottky-type structure, as evidenced by the significant difference in current under forward and reverse biases shown in Fig. 2c and Fig. 2f. It would be important to clarify whether the CdZnTe based device used for comparison in leakage current experiments also employed a Schottky-type structure. As seen in Fig. S9, the CdZnTe detector employs an Au/CdZnTe/Au. Without this information, the comparison may not be fair.

Response: Thank the Reviewer's question.

Firstly, the energy levels and n-type behavior of the CdZnTe material need to be taken into account in the choice of electrodes. The work functions of CdZnTe and Au are 4.3 eV and 4.7 eV, respectively. Moreover, the interface barrier height was determined to be 1.17 eV for Au-CdZnTe with passivation[3, 7]. Therefore, the Au/CdZnTe contact is a Schottky type[8]. The current curve also shows that the Au/CdZnTe contact is a Schottky contact, as shown in Fig. R11. Another significant feature of the Au/CdZnTe/Au detector is that the Au electrode serves as the charge collection contact, which can also be beneficial in fabricating detectors with pixel or coplanar-grid detectors from the current CdZnTe technology[9]. Secondly, both the single Schottky-type Sn/$CsPbBr_3$/Au and the double Schottky type Au/CdZnTe/Au detectors are in the same voltage-mode. Therefore, a comparison of $CsPbBr_3$ Schottky detector with commercial CdZnTe double-Schottky detector is reasonable and appropriate.

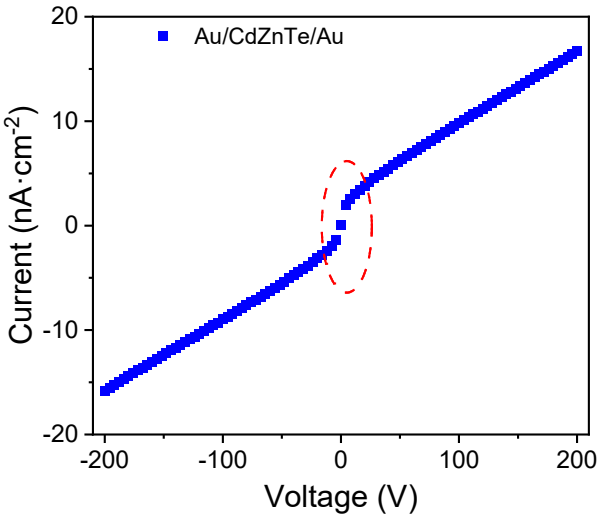

Fig. R11 *I-V* curve of Au/CdZnTe/Au device

8. “the detector is much thick” should be “the detector is much thicker”.

“the contribution of electrons to charge can be ignored when the radiation source is incident from the anode electrode (Fig. S7),” The direct line depicted in Fig. S7 suggests a simplistic model. It would be beneficial for the authors to elaborate on the methodology or formulae used to derive this relationship, as various factors such as interface defects, crystal imperfections, and the actual behavior of charge carriers in the presence of an electric field could significantly influence this contribution.

Response: Thank the Reviewer for providing helpful suggestions. We have revised “the detector is much thick” to “the detector is much thicker”.

In 1938, Shockley[10] and Ramo[11] calculated the Shockley-Ramo principle, *i.e.*, in a parallel-plate capacitor with 1 V applied to one electrode and the other electrode grounded, the light enters the carriers formed at a depth of x, as shown in Fig. R12. The induced charge generated on the detector pole plate when the carriers move satisfies:

$$Q(x)=\frac{q}{d}\left\{\int_0^x N_e(x)\,dx_e+\int_x^d N_h(x)\,dx_h\right\} \tag{1}$$

where x is the position from the electrode that the ionizing radiation is incident on, d is the thickness. Assuming that the capture centers are uniformly distributed in the crystal and that the carrier transport lifetime is sufficiently long, the number of carriers are:

$$N_e(x)=N_0\exp\left(-\frac{x}{(\mu\tau)_e E}\right) \tag{2}$$

$$N_h(x)=N_0\exp\left(-\frac{d-x}{(\mu\tau)_h E}\right) \tag{3}$$

Where N_0 is the initial number of the electron-hole pairs, which is determined by the E_{pair}, and the $\mu\tau$ product for holes (h) and electrons (e) are specified. The ratio of the induced charge to the initial charge Q_0 is defined as the charge collection efficiency η (Charge Collection Efficiency, CCE):

$$\eta = \frac{Q(x)}{Q_0} = \frac{(\mu\tau)_e}{d}\left(1-\exp\left(\frac{-x}{(\mu\tau)_e E}\right)\right)+\frac{(\mu\tau)_h}{d}\left(1-\exp\left(\frac{x-d}{(\mu\tau)_h E}\right)\right) \quad (4)$$

The contribution of electrons to charge can be ignored when the radiation source is incident from the anode electrode due to the depth of incidence of alpha particles is only a few tens of um (Fig. R9). Therefore, the CCE for the α-particle induced pulse height spectrum of the p-type perovskite detector is calculated using the Hecht equation [12]:

$$\eta \approx \frac{\mu\tau E}{d}\left(1-\exp\left(-\frac{d}{\mu\tau E}\right)\right) \quad (5)$$

It is worth noted that the Hecht equation is applicable when the electric field and the traps are distributed uniformly throughout the detector. Exactly, various factors such as interface defects, crystal imperfections, and the actual behavior of charge carriers in the presence of an electric field can significantly influence the CCE. For example, materials with low trap density are also advantageous, which is beneficial for charge collection. Moreover, the thickness of the depletion region in semiconductor detectors plays a role in charge collection, which dominates the carrier drift time. The charge cloud diffusion, which usually determines the trapping probability by the structure defects, is correlated with the carrier drift time. However, it is difficult to derive a special formula for the charge collection of a given defect from radiation detectors.

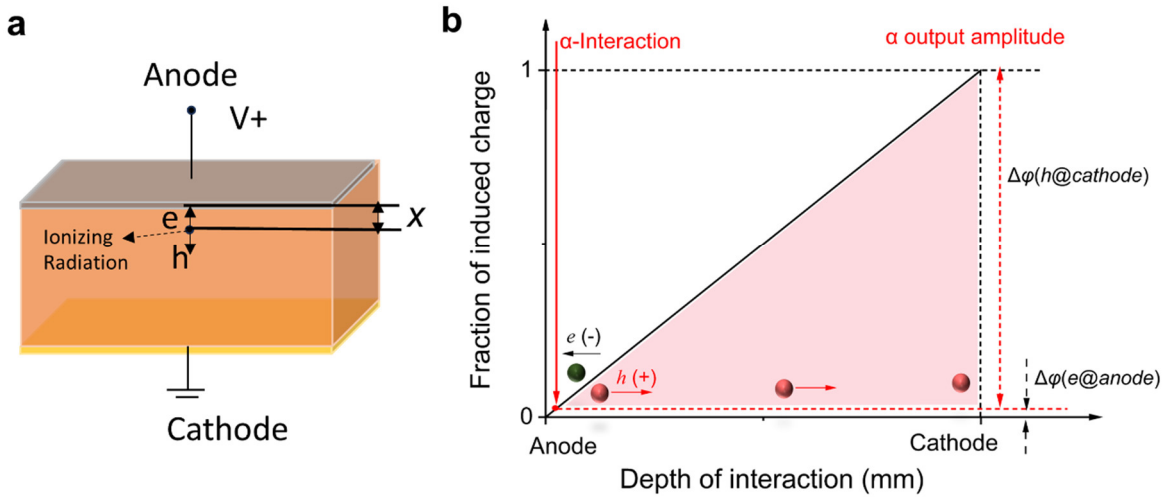

Fig. R12 Depth dependent charge sensing: (a) Detector with planar electrodes B) Signal contributions from holes and electrons in an ideal detector.

Changes in SI: Fig. R12 is added as Supplementary Fig. 9, and the relative formulate has been added in the Supplementary.

9. The authors have conducted numerous tests in vacuum conditions without specifying the operational details on how the vacuum was achieved. The difference in mobility values obtained in air and vacuum (42 $cm^2 \cdot V^{-1} \cdot s^{-1}$ and 49 $cm^2 \cdot V^{-1} \cdot s^{-1}$, respectively) is not substantial. Are these values measured from the same device in different environments or from separate devices tested in each condition?

Response: We used a special vacuum system for alpha particle experiments with a vacuum level of 4.5-5.0 Pa. The test equipment is shown in Fig. R13.

All these mobility values were measured with the same device. The hole mobility is an inherent property and independent on the environment. However, the path of low-angle particles along the detector is longer than that of incident particles, resulting in a greater probability of interaction with absorbing layers and air between the source and the detector. Thus, the hole mobility is degraded since the particles lose energy through interaction with air. The hole mobility values are similar in air and vacuum because the detector is closer to the radioactive source.

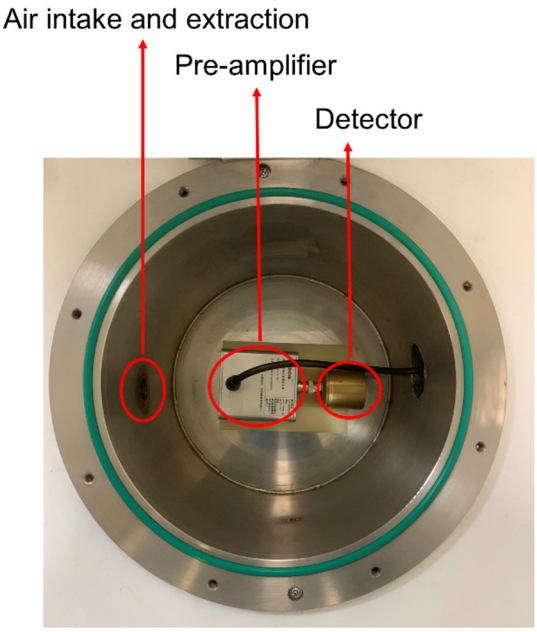

Fig. R13 The vacuum equipment.

Change in manuscript: "A specialized vacuum system for experiments measurement of alpha particle with a vacuum level of 4.5-5.0 Pa."

10. The authors have characterized the high-temperature stability of the device by analyzing the rise time distribution at various temperatures (Fig. 3e). However, the rise time distribution at room temperature already exhibits considerable variability, which raises questions about the intrinsic stability of the device or the consistency of the α-source. Given the known issues with perovskite response drift and instability during long-term storage, especially when using Sn electrodes prone to oxidation, it is imperative that the authors conduct further tests focused on the robustness and stability of the detector over prolonged periods.

Response: We Thank the Reviewer for providing helpful suggestions. We conducted long-term stability tests on the same sample. The stability can be divided into two parts, and the result were added in the revised manuscript.

(1) The stability of $CsPbBr_3$ detector operated under continually bias

To investigate the operation stability, the planar Au/$CsPbBr_3$/Sn detector was placed in air at room temperature. The polarization effect caused by ion migration and charge trapping, which results in spectrum shift and resolution degradation, is a major concern for the halide perovskites radiation detectors. The dark current of the Sn/$CsPbBr_3$/Au detector as a function of time was measured. It exhibits a small fluctuation under the reverse bias from 2 V to 200 V (Fig. R14 (a)), which demonstrates the better stability of the $CsPbBr_3$ detector with Schottky electrode.

After that, the detector was exposed to radiation from uncollimated ^{241}Am@5.5 MeV alpha particles for a period of time to obtain the response spectrum of the detector, with an applied electric field of 1000 V·cm^{-1} and a shaping time of 6 us. The number of peak channel numbers and the energy resolution were almost unchanged through continuous testing under 1000 V·cm^{-1} for 60 min for a detector exposed to alpha particles (Fig. R14 (b)), demonstrating the excellent stability of this material under large biases and high-energy particles. Further, we also measured the spectral response over a period of 12 hours at two-hour intervals, as shown in Fig. R15, which was added in manuscript as Fig. 4f.

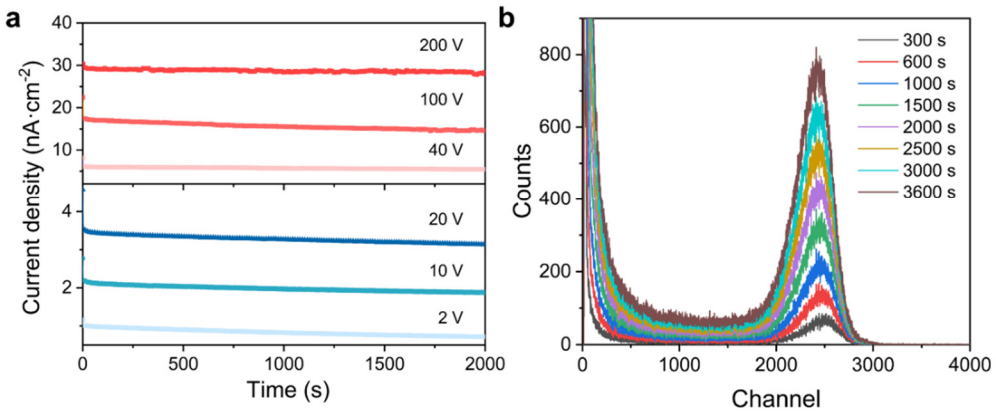

Fig. R14 Voltage stability of $CsPbBr_3$ devices. (a) Current density as a function of time at different biases. (b) Spectra with different collection time.

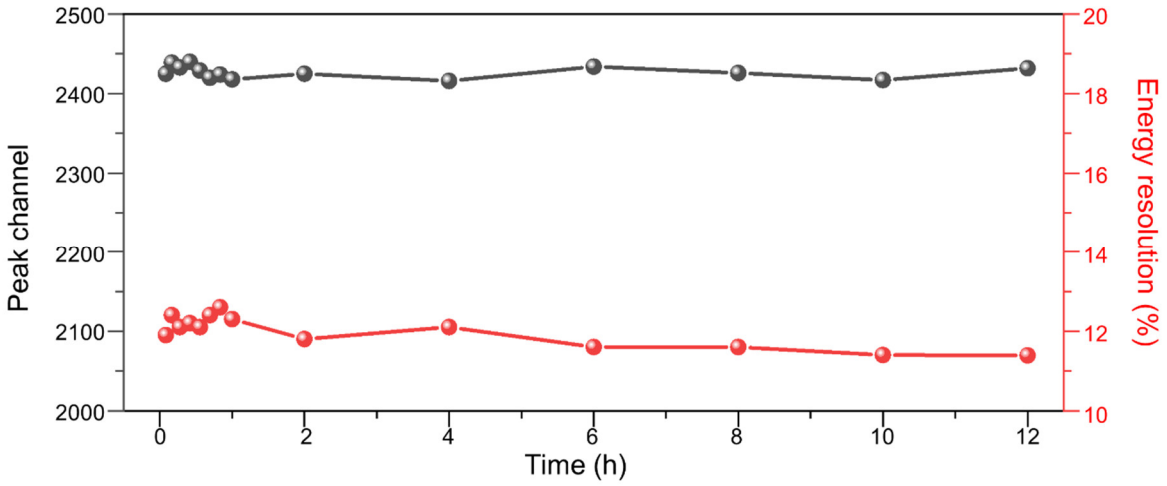

Fig. R15 The spectral response over a 12-hour period

(2) Storage stability of the $CsPbBr_3$ detector

The Au/$CsPbBr_3$/Sn detector demonstrates great long-term stability, as shown in Fig. R16. After nine months of storage in air without any encapsulation, the detector can still acquire the ^{241}Am@5.5 MeV alpha particle spectrum with the same peak number and energy resolution, which implies no degradation of devices and the electrode interfaces.

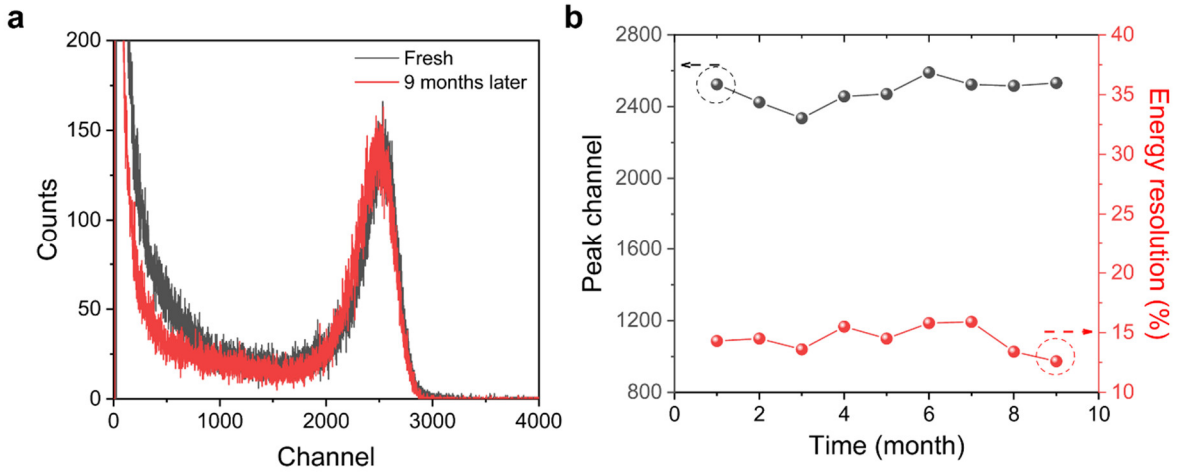

Fig. R16 (a) Spectrum collected at air for the fresh device and after nine months of storage. (b) The channel number and energy resolution from the testing spectrum biased at -100 V for nine months.

Change in manuscript: Fig. R15 is added as Fig. 4f.

"Generally, the polarization effect induced by ion migration and space charge resulting from $CsPb_2Br_5$ defects poses a significant concern for halide perovskites utilized in radiation detection, which leads to a shift of the full energy peak and deterioration of resolution[33]. The peak channel number and energy resolution maintain relative stability for the Sn/$CsPbBr_3$/Au detector exposed to alpha particles during a continuous test under 1000 V·cm^{-1} (shaping time was 6 μs) over 12 hours (Fig. 4f and Fig. S15). In addition, the pulse height spectra of the resulting unencapsulated $CsPbBr_3$ detector show small fluctuations for over 9 months (Fig.

S16), which demonstrates the promise of robustness and stability over prolonged periods."

Change in SI: Fig. R14 is added as Supplementary Fig. 15, Fig. R16 is added as Supplementary Fig. 16.

11. Could the authors clarify whether the 1.1% energy resolution was achieved under vacuum conditions?

Response: The energy resolution of 1.1% was achieved by a $CsPbBr_3$ detector with a full-customized readout ASIC under ambient conditions. Considering the practical application for charge particles (α/β), such as nuclear safety, homeland security, nuclear waste disposal, uranium mining, smelting and processing, decommissioning sites of nuclear facilities, radiochemical analysis laboratories, reactor halls, and nuclear power plant buildings[13-15], high performance detection in air is more difficult and demanding than in vacuum.

The relative test conditions "under ambient conditions" have been added in the revised manuscript.

12. Y. H. et al. achieved an energy resolution of 1.4% for γ-particle detection using the same $CsPbBr_3$ material in 2021 (*Nat. Photon.*, 15, 36-42(2021)), comparable to the energy resolution for α-particle detection in this work. Given the typically more complex interaction pathways and broader energy spectrum of γ-particles, achieving finer energy resolution is more challenging for γ detection than for α detection. Therefore, the breakthrough significance of this work appears limited.

Response: Thank the Reviewer's comments. It is great progress that Y. H. et al. achieved an energy resolution of 1.4% with depth correction for ^{137}Cs 662 keV γ-rays using $CsPbBr_3$ grown by the Bridgeman method[16], which was also cited in our manuscript. However, it is important to note that high-energy particles detection is significantly different from gamma-rays detection in the following ways:

(1) Alpha particles react strongly with matter because of they are comparatively heavy and have a charge that generates a large number of ions per unit length of their path. As a result, they are not very penetrating. For example, 5 MeV alpha particles only penetrate about 3.6 cm in air and do not penetrate an ordinary piece of paper, resulting in performance that will be severely affected by defects in the surface interface and the electrodes.

(2) Alpha particles are strongly scattered in air, which undoubtedly loses energy and leads to a broadening of the half-peak width, and makes high energy resolution in air much harder. This also presents additional challenges to the quality and charge collection efficiency of the detector compared to γ-ray detection.

(3) the Fukushima nuclear accident in Japan alerts that the monitoring of radioactivity in the air has gained extensive attentions throughout the world. One of the main tasks of government organized emergency tests was to detect the radioactivity of aerosols in the environment. Currently, these tests mainly focus on α and β particles, which is applied to uranium mining, smelting and processing, decommissioning site of nuclear facilities,

monitoring of reactor hall and nuclear power plant, et. al. Thus, our high energy resolution of perovskite single-crystal detector is urgently for alpha particle detection.

Therefore, based on our results and the work reported by Y.H. et al., we believe the $CsPbBr_3$ detectors have broad application in radiation detection fields, not only for X- and γ-rays, but also for high energy particles.

Reviewer #3 (Remarks to the Author):

This work by Zhang et al demonstrated an alpha particle detector with high energy resolution below 1.1%. By thinning the $CsPbBr_3$ crystal, they improved the crystal quality by removing the unwanted phase and extended defects, and thus a low dark current. They have characterized the carrier mobility, trap density of the thinned crystal to validate this point. Finally, they have investigated the alpha-particle detection performance with their device in great details. While the demonstrated performance is highly promising, the main concern is the poor material innovation of this work which does not warrant the publication in a high profile journal like Nature Comm. Simply thinning the crystal yields very little control over the final product. If the crystal defects are located all through the bulk, this method would not be applicable anymore. In other words, the main finding or method of this work is not broadly applicable to other perovskite crystal system. Its potential impact could be very limited. I hesitate to recommend its publication in Nature Comm in its current format.

Response: Thank the Reviewer's comments. We have made modifications and supplementary explanations in the revised manuscript.

Our work is not limited to materials, but also involves detector preparation, nuclear electronics (microelectronics) and nuclear testing technology, which is a comprehensive and multidisciplinary work. In addition, the innovation involved and the reference effect for other work are summarized as follows:

(1) Single-crystal perovskite materials have shown broad prospects in the field of photoelectric detection. The polishing process is the basis for subsequent applications, but due to the special water and oxygen sensitivity of perovskite, traditional semiconductor polishing is no longer suitable (polishing of water solutions). In this manuscript, we propose a polishing process applicable to single-crystal perovskite, which has a reference value for other perovskite crystals, such as $FaPbBr_3$, $MAPbBr_3$ and $CsPbBr_3$ single crystals[17, 18]. And the thinning technology has a reference for all perovskite grown by solution methods, since the perturbation of the local temperature and solution concentration is inevitable.

(2) Due to the special transport properties of chalcogenides (long drift times), ballistic deficits will occur when commercial electronic systems are used. We propose a new ASIC system for perovskites to reduce the ballistic deficit, which matches well with the given parameters of the $CsPbBr_3$ detector and improves the performance. Compared to the current circuit designs mainly aimed at Si and CdZnTe, the ASIC design concept in this manuscript has reference value for other perovskite semiconductor detectors.

(3) We have conducted stability experiments closer to operating conditions, which is of great significance for promoting the application of perovskite detectors. After nine months of storage in air without any encapsulation, the detector still shows no significant change in the peak channel number and energy resolution of the ^{241}Am@5.5 MeV α particle spectrum.

The specific modifications will be discussed item-by-item later.

The detailed technical comments are listed below:

1. **(a)** The improvement by the thinning method is not well understood. It is not clear why $CsPb_2br_5$ would be the unwanted phase. If it's an insulator phase, it should not contribute to the dark current. **(b)** It is also not clear what type of extended defects are there at the surface, and why could thinning remove them without causing other types of surface defects?
Response: Thank the Reviewer's question. The question can be divided into two parts.

Question (a): Firstly, although both the $CsPb_2Br_5$ phases and the $CsPbBr_3$ matrix are semiconductors with a relatively wide bandgap, the crystal structure of $CsPbBr_3$ grown by the low-temperature solution method is three-dimensional, while $CsPb_2Br_5$ is a two-dimensional layered structure (Fig. R17)[19]. This leads to the fact that the coexistence of $CsPb_2Br_5$ with $CsPbBr_3$ was considered as a heterojunction distributed in the crystal along the thickness gradient[1, 2]. In addition, although the reaction diffusion between the crystal and the electrode can be reduced by optimizing the thickness of the intermediate layer and the preparation process, the existence of the interface will have an impact on the charge collection.

Secondly, the lattice mismatch density is higher at the two-phase interface, and the high density of suspension bonds weakens the carrier binding effect on the atoms at the interface, leading to a higher concentration of non-equilibrium carriers than in other regions. In addition, this also leads to the enrichment of defects such as impurities, dislocations *et.al.*, thus introduces more non-equilibrium carriers, which similar results were reported by literatures[20, 21]. These defects are easy to capture the charge at the interface, resulting in the reduction of charge collection efficiency.

For the above reasons, the $CsPb_2Br_5$ phase particles affect the dark current.

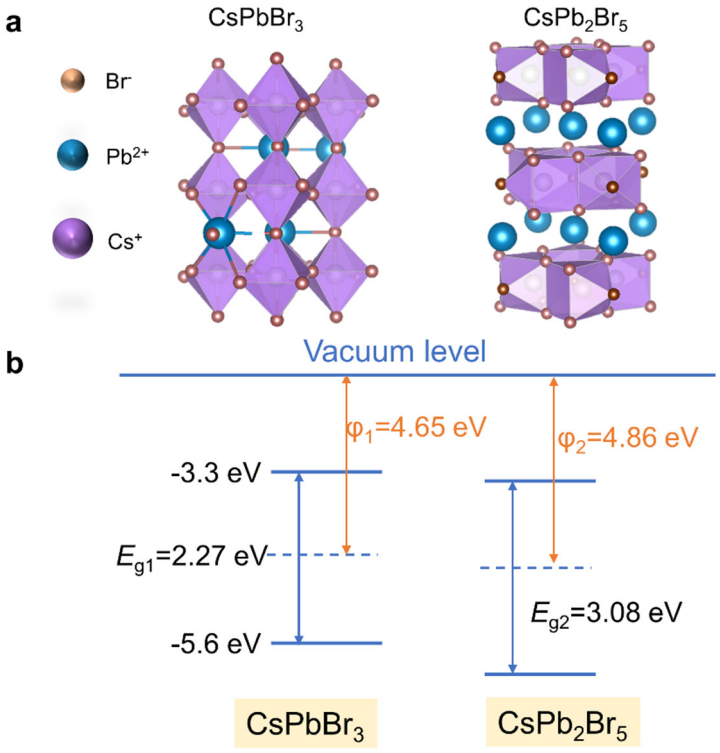

Fig. R17 Crystal structure schematic of (a) $CsPbBr_3$, and $CsPb_2Br_5$ at room temperature. (b) The energy band structure diagram of the contact between $CsPbBr_3$ and $CsPb_2Br_5$.

Change in manuscript: Fig. R17 (a) is added as Fig. 2b.

"Although the two-dimensional $CsPb_2Br_5$ secondary phase has a wider bandgap than the three-dimensional $CsPbBr_3$ (Fig. 2b), the charge transport properties are usually degraded by the misfit interface and the extended defect[35, 36]. The free carrier concentration, which dominates the bulk resistivity, is significantly affected by the grown-in point defects and impurities that accumulate at the interface[35]. To investigate the effects of the $CsPb_2Br_5$ defects, the electrical performance of $CsPbBr_3$ crystals was characterized."

Question (b): Due to the limitation of the growth method, the deviation of the precursor solution continually changes during the crystallization, and the $CsPb_2Br_5$ phase is inevitably formed. Additionally, the mismatching stress between the $CsPb_2Br_5$ phase and the $CsPbBr_3$ crystal leads to an enrichment of point defects around the $CsPb_2Br_5$ phases[22]. At the same time, with the progress of crystal growth, the density of $CsPb_2Br_5$ gradually increases because the precursor solution concentration deviates from the ideal value, and the density is the highest density on the crystal surface. Therefore, removing the near-surface by thinning is beneficial to reducing the overall defect density of the crystal.

The macro defects of the surface were eliminated by polishing and thinning. There is no impact on the performance results even if other types of surface defects are introduced in the thinning process (Fig. 2c and Fig. R18) by X-ray rocking curve and *I-t* tests.

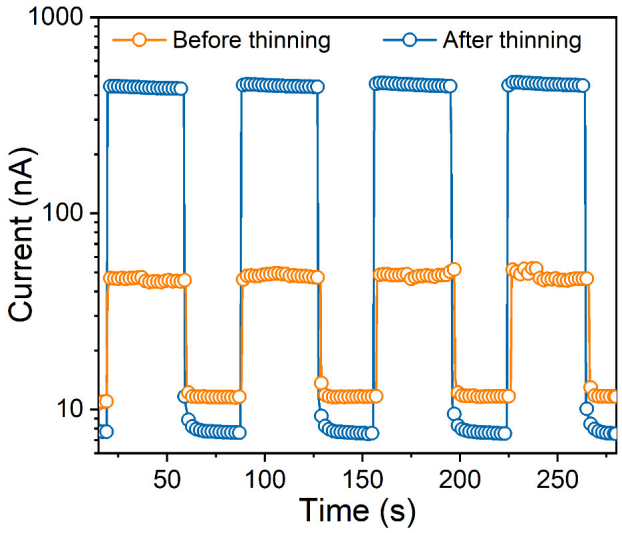

Fig. R18 I-t curves before and after thinning at -50 V.

2. From the current discussion, it is not clear why Sn/perovskite interface is stable as SnO peaks were observed at the interface. Literature studies cited by the author also suggested that Sn can diffuse into the perovskite structure causing instability. And what is special in this case that makes the interface stable?

Response: According to the XPS results, the chemical states of Sn can be attributed to metallic and ionic states, as shown in Fig. R19. The peak at 485.6 eV is attributed to the oxidation of Sn, and the peak at 486.7 eV is attributed to the formation of the Br-Sn compound. As the etching depth increases, the proportion of Br-Sn gradually increases, while the proportion of Sn-O decreases gradually. These prove that an inevitable chemical reaction

has occurred between Sn and the $CsPbBr_3$ single[18, 20]. To further determine the extent of the reaction, an analysis of the chemical state of Pb at the interface was conducted, as shown in Fig. R20. The ratio of the peak areas of Pb^0 and Pb^{2+} was fitted to quantify the extent of the reaction between metal and $CsPbBr_3$[5]. The corresponding redox equations are presented as follows:

$$Pb^{2+} + 2e^- = Pb^0$$

The Pb^0/Pb^{2+} of Sn and $CsPbBr_3$ devices is 0.14. Compared with the reference[5], this ratio is the same as that of the optimized Au/Al/BCP/C_{60}/$CsPbBr_3$/Au structure, which is used to suppress ion migration and interface electrochemical reactions. Thus, there is a stable contact with negligible reaction between Sn and $CsPbBr_3$.

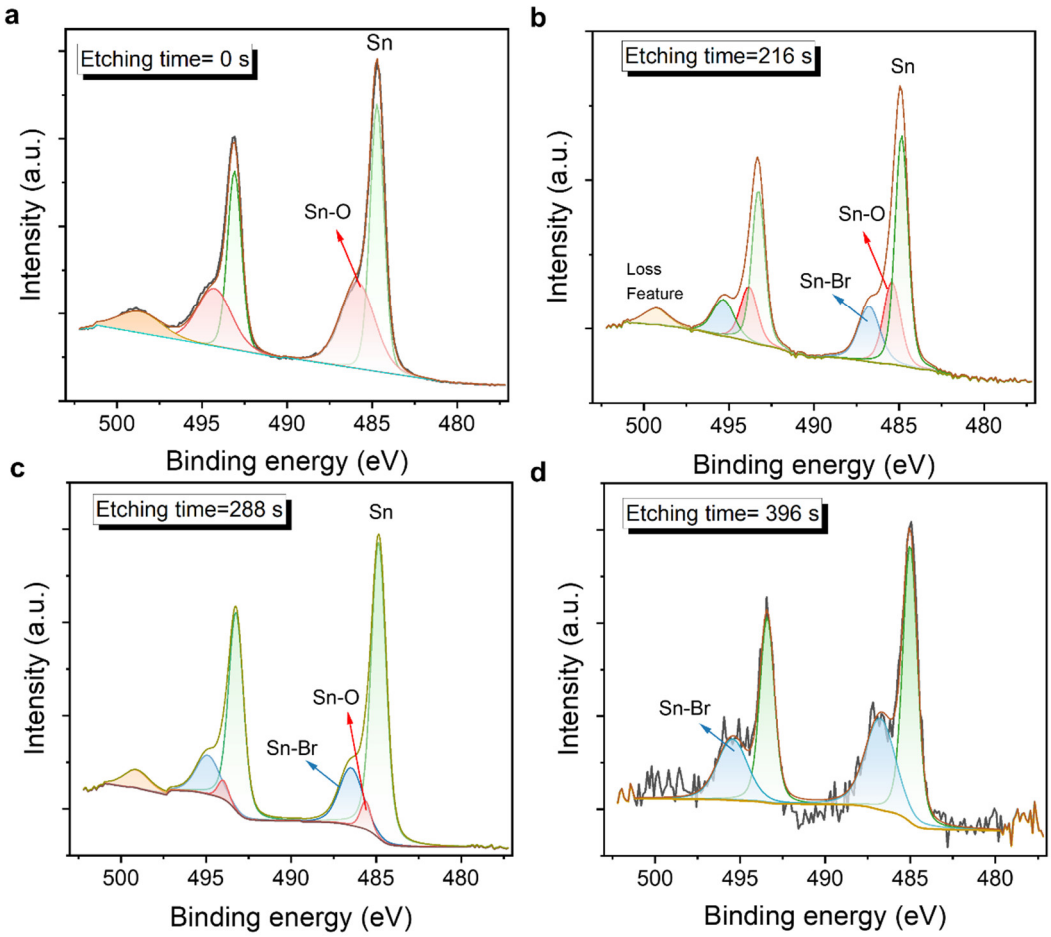

Fig. R19 X-ray photoelectron spectroscopy (XPS) measurements with different eating time. (a) 0 s. (b) 216 s. (c) 288 s. (d) 396 s.

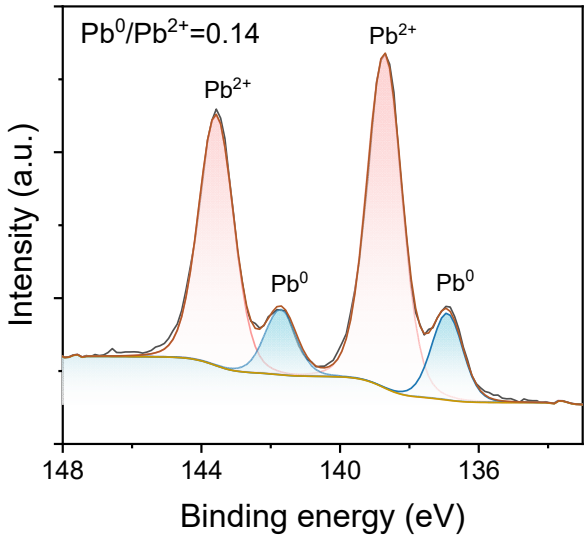

Fig. R20 The XPS results of Pb elements of Sn and $CsPbBr_3$.

Change in manuscript: Fig R 19 (d) is added as Fig. 2f. Fig. R20 is added as Fig. 2g.

"In addition, the chemical state of Sn at the interface was determined, which showed a weak Sn-Br peak at 486.74 eV (Fig. 2f), indicating an inevitable reaction[38, 40]. To quantify the reaction, the peak area ratio of Pb^0 and Pb^{2+} is fitted according to the corresponding redox equation[39, 42, 43]:

$$Pb^{2+} + 2e^- = Pb^0 \quad (2)$$

The Pb^0/Pb^{2+} ratio is 0.14 for Sn/$CsPbBr_3$/Au (Fig. 2g), that is comparable to the optimized Au/Al/BCP/C_{60}/$CsPbBr_3$/Au structure[42], which demonstrate a stable contact with negligible reaction between Sn and $CsPbBr_3$."

Change in SI: Fig. R19 (a)-(c) is added as Supplementary Fig. 6.

3. The extremely slow rise time of the $CsPbBr_3$ detector is not understood in Fig. 4a-b. **(a)** There is a long tail near the slower side (100 us) which persist at higher bias (40 us). How is the rise time compared to other perovskite crystals, and **(b)** what's the impact of crystal thinning on the rise time? **(c)** And why would higher temperatures narrow the rise time distribution?

Response: Thank the Reviewer's question. The question can be divided into three parts.

Question (a): Based on the present study, the rise time of other perovskites is summarized in Table R3. The reason that the rise time at high pressure also has a long tail is that to ensure the accuracy of the measurement, a minimum of 1000 traces were collected for the statistics. The carriers, which drift slowly due to the trapping and de-tapping effect by structure defects, lead to a longer collection time, which results in a broadening of the full-energy peak in the pulse height spectrum.

Table R3 The rise time of perovskite single crystal

Materials	Growth method	Electric field ($V \cdot cm^{-1}$)	Rise time (μs)	Refs.
$Cs_3Sb_2I_9$	Bridgman	2325	10	[23]
$CsPbBr_3$	Bridgman	900	3	[24]
$CsPbBr_3$	Solution	---	~20	[25]
$FAPbBr_3$	Solution	231	15	[17]
$(BDA)CsPb_2Br_7$	Solution	250	12	[26]
$MAPbBr_3$	Solution	500	~50	[27]
$MAPbBr_{2.85}Cl_{0.15}$	Solution	250	20	[28]

Question (b): The $CsPb_2Br_5$ phase with a high concentration on the crystal surface decreases the carrier mobility and increases the carrier drift time. The rise time of before and after thinning are 10.01 μs and 2.54 μs, respectively, as shown in Fig. R21.

The existence of high-density extended defects enriched in the incoherent interface surrounding $CsPb_2Br_5$ phases tends to act as trapped centers, ultimately affecting the charge carrier drift time and carrier mobility. Moreover, the interfaces between the $CsPb_2Br_5$ defects and the overall spatially heterogeneous three-dimensional distribution of the substrate in the sample destroy the lattice periodicity, build up the barrier for charge carrier transport and form channels for ion migration[29]. Therefore, the existence of $CsPb_2Br_5$ phases increases the carrier transport time and reduces the carrier mobility of the detector.

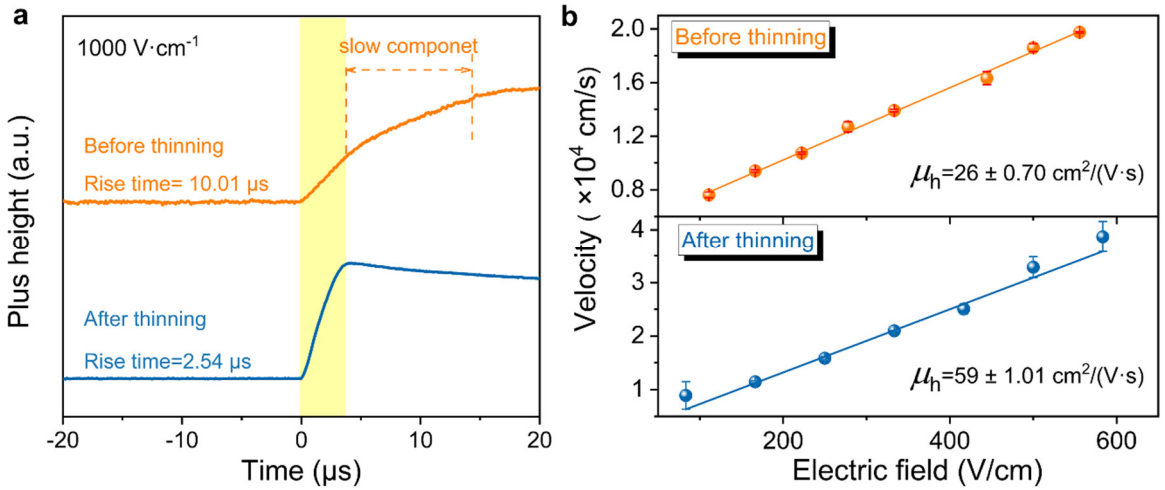

Fig. R21 The influence of thinning the crystal on carrier transport. (a) Carrier mobility by linear fitting for before and after thinning. (b) α particle induced pulse shapes and the rise time under the same electric field strength (1000 $V \cdot cm^{-1}$) for before and after thinning.

Question (c): The detector operates in pulse mode, such that each radioactive event is collected and processed individually. Therefore, the charge transport properties can be extracted based on the statistical analysis of the raw transient pulses. Fig. 4e shows a statistical distribution of a total of 1000 traces used to calculate the average drift time. The

half peak width of the distribution varies due to statistical fluctuations. Lattice scattering increasing as the temperature increase, which lead to a longer rise time. The Gaussian fit shows that the rise time at the central peak increases from 3.5 us at room temperature to 5.5 us at 343 K. The smaller fluctuation in rise time is due to the wide bandgap, resulting in the scattering to be insensitive to the temperature increase.

Change in manuscript: "Note that all experiments were performed after the $CsPbBr_3$ crystal was thinned and polished since the $CsPb_2Br_5$ phases affect the rise time and mobility of the detector (Fig. S13)."

Change in SI: Fig. R21 is added as Supplementary Fig. 12.

4. The operational stability (under irradiation and under electrical field stress) should be measured.

Response: We Thank the Reviewer for providing helpful suggestion.

(1) The stability of $CsPbBr_3$ detector operated under continually bias

Firstly, the dark current of the Sn/$CsPbBr_3$/Au detector as a function of time was measured. It exhibits a small fluctuation under the reverse voltage from 2 V to 200 V (Fig. R22), which demonstrates the better stability of the $CsPbBr_3$ detector with Schottky electrode. The detector was then exposed to radiation of uncollimated ^{241}Am@5.5 MeV alpha particles for a period of time to obtain the response spectrum of the detector. The test conditions were an applied electric field of 1000 $V \cdot cm^{-1}$ and a shaping time of 6 us.

It can be seen that the peak channel number and the energy resolution were almost unchanged through continuous testing under 1000 $V \cdot cm^{-1}$ for 60 minutes for a detector exposed to alpha particles, demonstrating the excellent stability of this material under large biases and high-energy particles. Further, we measured the spectral response over a at two-hour intervals 12-hour period (Fig. R23).

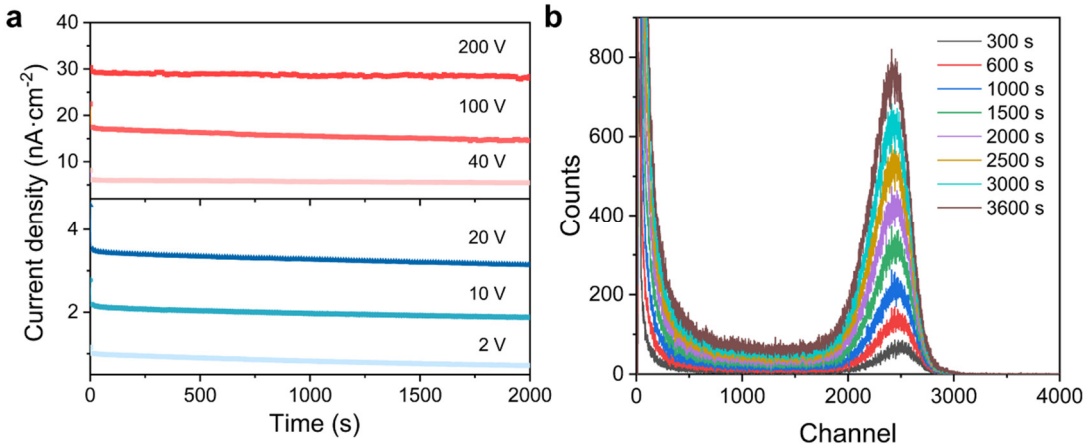

Fig. R22 Voltage stability of $CsPbBr_3$ devices. (a) Current density as a function of time at different biases. (b) Spectra with different collection time.

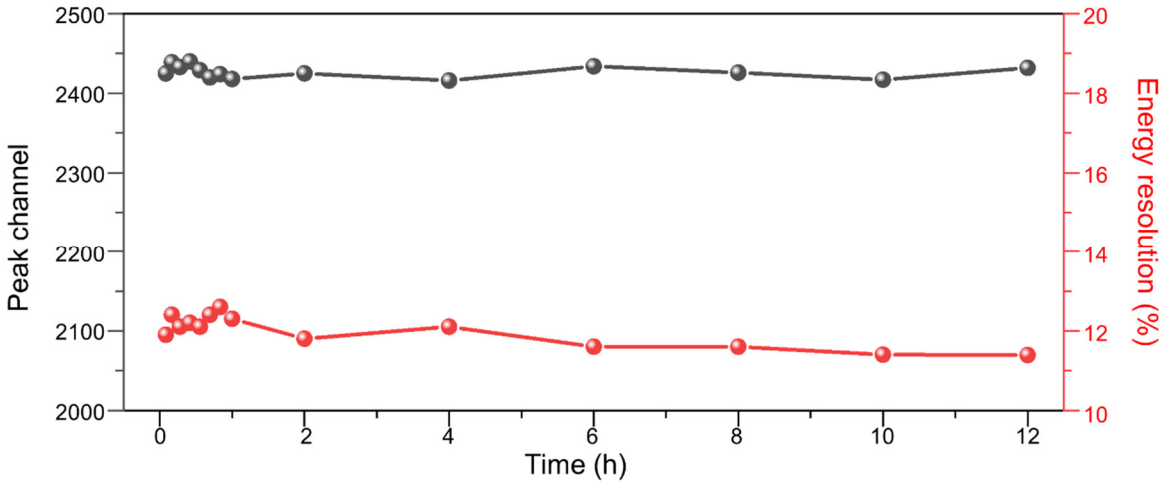

Fig. R23 The spectral response over a 12-hour period.

(2) Storage stability of the $CsPbBr_3$ detector

The spectra collected by Au/$CsPbBr_3$/Sn detector obtained under irradiation for the fresh device and after nine months are shown in Fig. R24. After nine months of storage in air without any encapsulation, the detector still has no significant change in the peak channel number and energy resolution of ^{241}Am@5.5 MeV α particle spectrum, which implies no degradation of devices and the electrode interfaces.

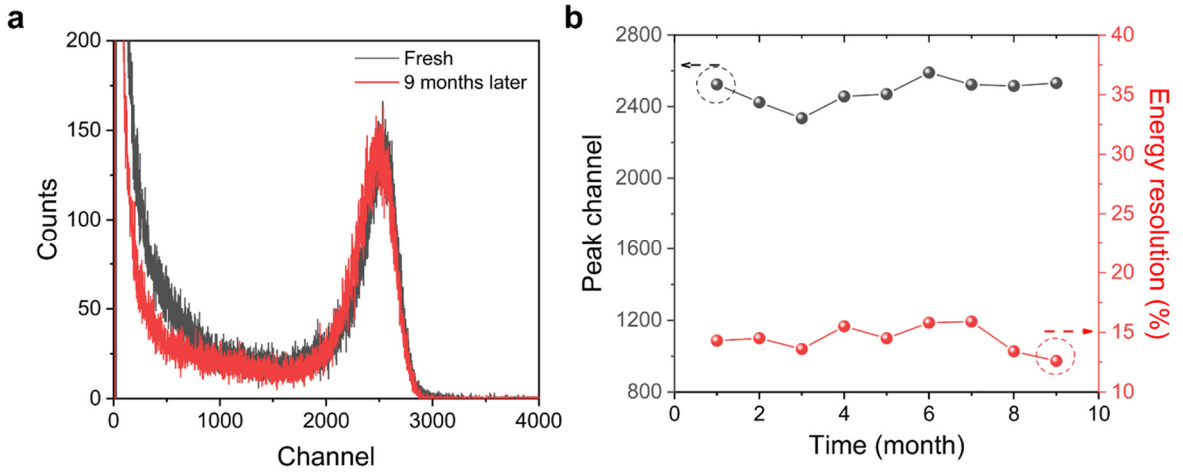

Fig. R24 (a) Spectrum collected at air for the fresh device and after nine months of storage. (b) The channel number and energy resolution from the testing spectrum biased at -100 V for nine months.

Change in manuscript: Fig. R23 is added as Fig. 4f.

"Generally, the polarization effect induced by ion migration and space charge resulting from $CsPb_2Br_5$ defects poses a significant concern for halide perovskites utilized in radiation detection, which leads to a shift of the full energy peak and deterioration of resolution[33]. The peak channel number and energy resolution maintain relative stability for the Sn/$CsPbBr_3$/Au detector exposed to alpha particles during a continuous test under 1000 $V \cdot cm^{-1}$ (shaping time was 6 μs) over 12 hours (Fig. 4f and Fig. S15). In addition, the pulse height spectra of the resulting unencapsulated $CsPbBr_3$ detector show small fluctuations for over 9 months (Fig.

S16), which demonstrates the promise of robustness and stability over prolonged periods."

Change in SI: Fig. R22 is added as Supplementary Fig. 15, Fig. R24 is added as Supplementary Fig. 16.

Reference

1. Cheng, Y., et al., Precursor solution-dependent secondary phase defects in $CsPbBr_3$ single crystal grown by inverse temperature crystallization. *J. Mater. Chem. A* **9**, 27718-27726 (2021).
2. Cheng, Y., et al., Secondary phase particles in cesium lead bromide perovskite crystals: an insight into the formation of matrix-controlled Inclusion. *J. Phys. Chem. Lett.* **11**, 5625-5631 (2020).
3. Prokesch, M.; Szeles, C., Accurate measurement of electrical bulk resistivity and surface leakage of CdZnTe radiation detector crystals. *J. Appl. Phys.* **100**, 014503 (2006).
4. Wu, S., et al., A chemically inert bismuth interlayer enhances long-term stability of inverted perovskite solar cells. *Nat. Commun.* **10**, 1161 (2019).
5. Chen, Z., et al., Ultrasensitive and robust $CsPbBr_3$ single-crystal x-ray detectors based on interface engineering. *ACS Appl. Mater. Interfaces* **15**, 51370-51379 (2023).
6. Hao, Y., et al., Investigation of LiF interlayer on charge collection efficiency and leakage current in $CsPbBr_3$ radiation detector. *IEEE T. Electron Dev.* **69**, 6837-6842 (2022).
7. Li, Q., et al., Investigation on interface barrier of Au-CdZnTe contacts. *Nucl. Instrum. Meth. A* ***564***, 544-548 (2006).
8. Yang, F., et al., A modified diffusion model for characterization of real I-V curve and charge collection efficiency of CdZnTe detectors. *Nucl. Instrum. Meth. A* **959**, 163515 (2020).
9. Yang, G., et al., Performance of common-grid pixelated CZT detector with different array geometries. *J. Instrum.* **10**, P06008-P06008 (2015).
10. Shockley, W., Currents to conductors induced by a moving point charge. *J. Appl. Phys.* ***9***, 635-636 (1938).
11. Ramo, S., Currents induced by electron motion. *Proceedings of the IRE* **27**, 584-585 (1939).
12. Hecht, K., Zum Mechanismus des lichtelektrischen primrstromes in isolierenden kristallen. *Zeitschrift fr Physik* **77**, 235-245 (1932).
13. Gorenstein, P.; Bjorkholm, P., Detection of radon emanation from the crater aristarchus by the Apollo 15 alpha particle spectrometer. *Science* ***179***, 792-794 (1973).
14. Povinec, P., et al., Aerosol radioactivity monitoring in Bratislava following the Chernobyl accident. *J. Radioanal. Nucl. Ch.* ***126***, 467-478 (1988).
15. García-Torao, E., et al., Alpha-particle emission probabilities in the decay of 239 Pu. *Nucl. Instrum. Meth. A* ***334***, 477-484 (1993).
16. He, Y., et al., $CsPbBr_3$ perovskite detectors with 1.4% energy resolution for high-energy γ-rays. *Nat. Photonics* **15**, 36-42 (2020).
17. Liu, X., et al., Solution-grown formamidinium hybrid perovskite $FAPbBr_3$ single crystals for alpha-particle and gamma-ray detection at room temperature. *ACS Appl. Mater. Interfaces* **13**, 15383-15390 (2021).
18. Liu, X., et al., Charge transport behavior in solution-grown methylammonium lead tribromide perovskite single crystal using α particles. *J. Phys. Chem. C* **122**, 14355-14361 (2018).
19. Li, M., et al., Synthesis of two-dimensional $CsPb_2X_5$ (X = Br and I) with a stable structure and tunable bandgap by $CsPbX_3$ phase separation. *J. Phys. Chem. Lett.* **13**, 2555-2562 (2022).
20. Almora, O., et al., Ionic charging by local imbalance at interfaces in hybrid lead halide perovskites. *Appl. Phys. Lett.* ***108***, 043903 (2016).
21. Shao, Y., et al., Grain boundary dominated ion migration in polycrystalline organic-inorganic halide perovskite films. *Energ Environ. Sci.* **9**, 1752-1759 (2016).
22. He, Y., et al., Dislocation-mediated coupling mechanism between the microstructural defects and Te

inclusions in CdZnTe single crystals. *Scripta Materialia* ***82***, 17-20 (2014).
23. McCall, K. M., et al., α-particle detection and charge transport characteristics in the $A_3M_2I_9$ defect perovskites (A = Cs, Rb; M = Bi, Sb). *ACS Photonics* **5**, 3748-3762 (2018).
24. He, Y., et al., Perovskite $CsPbBr_3$ single crystal detector for alpha-particle spectroscopy. *Nucl. Instrum. Meth. A* **922**, 217-221 (2019). He, Y., et al., Perovskite $CsPbBr_3$ single crystal detector for alpha-particle spectroscopy. *Nucl. Instrum. Meth. A* **922**, 217-221 (2019).
25. Bennett, S. H., et al., Charge transport comparison of FA, MA and Cs lead halide perovskite single crystals for radiation detection. *Front. Detect. Sci. Technol.* **1**, 1249892 (2023).
26. Xiao, B., et al., Towards superior X-ray detection performance of two-dimensional halide perovskite crystals by adjusting the anisotropic transport behavior. *J. Mater. Chem. A* **9**, 13209-13219 (2021).
27. Tisdale, J. T., et al., Precursor purity effects on solution-based growth of $MAPbBr_3$ single crystals towards efficient radiation sensing. *CrystEngComm* ***20***, 7818-7825 (2018).
28. Tisdale, J. T., et al., Methylammonium lead tribromide single crystal detectors towards robust gamma-ray photon sensing. *Adv. Opt. Mater.* **8**, 2000233 (2020).
29. Ding, J., et al., The role of surface defects in photoluminescence and decay dynamics of high-quality perovskite $MAPbI_3$ single crystals. *J. Phys. Chem. Lett.* **9**, 4221-4226 (2018).

REVIEWER COMMENTS

Reviewer #2 (Remarks to the Author):

I appreciate the authors' revisions as well as the detailed information added. However, I will not overturn my suggestion on the rejection of this manuscript, since the novelty and significance don't meet the critical standards of the high-quality Nature Communications journal. Detailed comments are listed below:

1. The CsPbBr3 detector has been repeatedly reported for radiation detectors. There is no breakthrough in the material design. Thinning the crystal thickness doesn't justify the novelty.
2. The energy resolution of 1.4% for γ photon detection is realized by the same CsPbBr3 material many times (Nature Photon., 15, 36 (2021)). I also thank the authors for their input in highlighting the difference between α-particle detection and γ photon detection. Unfortunately, the discussion didn't hit the nail on the head. It is true that "the α-particles are not very penetrating", and α-particles-induced charges are generated on the surface region of the bulk perovskite crystals. From this point of view, charges are more easily collected by the surface electrodes than the case for γ photon detection, since γ photon-induced charges are generated deep inside the crystals, and need to drift a long distance before collection or recombination. Considering the penetrating depth of tens of micrometers of α-particles, the perovskite layer (1 mm) in the manuscript is much too thick for high-efficiency energy conversion, as a fatal flaw in the design. The large thickness is not only a waste of material, but also detrimental for the charges collection. Just think about the high-efficiency perovskite solar cells, and a 1-micrometer perovskite layer is thick enough to fully absorb the sunlight, and we don't need a 100-micrometer perovskite crystal to ruin the efficiency.
3. The resistivity value is still derived out of the range of working bias...

Reviewer #3 (Remarks to the Author):

The authors have made good efforts addressing the comments, however, I'm not fully convinced by the discussion for the rise time distribution. It is not obvious from the discussion of why the distribution gets narrower because of the wider band gap. Much more detailed discussion is needed.

Response to Referees

Reviewer #2 (Remarks to the Author):

I appreciate the authors' revisions as well as the detailed information added. However, I will not overturn my suggestion on the rejection of this manuscript, since the novelty and significance don't meet the critical standards of the high-quality Nature Communications journal. Detailed comments are listed below

Response: We appreciate the comments on our work from the reviewer, which are essential for improving the quality of this manuscript. *Nature Communications* is a multidisciplinary journal that publishes high-quality research from all areas of the natural sciences. In addition to material design, *Nature Communications* also focuses on integrated circuit, algorithm optimization, and detector design. For example, Tobias J. Kippenberg (*Nat. Commun.* **15**, 3134, 2024) reported the photonic-electronic integrated circuit. Alejandro Perdomo-Ortiz (*Nat. Commun.* **15**, 2761, 2024) reported an optimization combinatorial with classical and quantum generative models. Guangda Niu (*Nat. Commun.* **15**, 1769, 2024) presented a scheme of in-X-ray-detector computing. Therefore, we believe that this work involves interdisciplinary collaboration and is highly suitable for the scope and purpose of *Nature Communications*. And we have carefully revised the manuscript and given the responses point by point according to the comments.

1. The $CsPbBr_3$ detector has been repeatedly reported for radiation detectors. There is no breakthrough in the material design. Thinning the crystal thickness doesn't justify the novelty.

Response: We thank the reviewer for carefully reading our manuscript and providing the comments. The main innovation of this research is that our interdisciplinary work focuses primarily on improving the energy resolution of $CsPbBr_3$ detector for α-particle, involving crystal materials, device processing, and readout electronics. Specifically, this is reflected in the following aspects:

(1) Firstly, it is currently difficult to achieve higher energy resolution for α-particle only through material design. Mercouri G. Kanatzidis[1] demonstrated that $CsPbBr_3$ devices resolve ^{137}Cs 662-keV γ-rays with 1.4% energy resolution by optimizing material, electrodes, and depth-correction algorithm (*Nat. Photonics* **15**, 36, 2020). More importantly, the highest resolution of the reported perovskite detector for α-particle is only 5.7%[2], which does not meet application standards. Therefore, although the $CsPbBr_3$

detector has many reports on radiation detectors, there has been no breakthrough in the energy resolution of α-particle.

(2) From the aspect of application, an excellent radiation detector module is a long-term work, the key factors include the crystal material, detector processing, and matching the electronic design. In our manuscript, we matched the optimized $CsPbBr_3$ detector to the electronics and achieved the highest energy resolution for α-particle. Such performances have not been achieved in perovskite single crystal-based detectors before. We believe that it was achieved not only due to material design but also related to device and electronics design, which justifies the novelty and significance of our manuscript. This innovation provides valuable insights for the development of perovskite α-particle detector in both academic and practice application.

Changes in manuscript: In order to highlight the innovation of our manuscript, we modify the title as "High energy resolution $CsPbBr_3$ detector with a full-customized readout ASIC for alpha particle detection". We have also made appropriate changes in the Introduction.

2. The energy resolution of 1.4% for γ photon detection is realized by the same $CsPbBr_3$ material many times (*Nature Photon.*, 15, 36 (2021)). I also thank the authors for their input in highlighting the difference between α-particle detection and γ photon detection. Unfortunately, the discussion didn't hit the nail on the head. It is true that "the α-particles are not very penetrating", and α-particles-induced charges are generated on the surface region of the bulk perovskite crystals. **(a)** From this point of view, charges are more easily collected by the surface electrodes than the case for γ photon detection, since γ photon-induced charges are generated deep inside the crystals, and need to drift a long distance before collection or recombination. **(b)** Considering the penetrating depth of tens of micrometers of α-particles, the perovskite layer (1 mm) in the manuscript is much too thick for high-efficiency energy conversion, as a fatal flaw in the design. The large thickness is not only a waste of material, but also detrimental for the charges collection. Just think about the high-efficiency perovskite solar cells, and a 1-micrometer perovskite layer is thick enough to fully absorb the sunlight, and we don't need a 100-micrometer perovskite crystal to ruin the efficiency.

Response: Thank the Reviewer's question. The question can be divided into two parts.

Question (a): Although the α-particles-induced charges are generated on the surface region of the bulk perovskite crystals, the incident and collection electrodes are opposite, as shown in Fig. R1 (a). **Consequently, holes must traverse essentially the entire length of the crystal, implying that charge carriers drift a longer distance before collection compared**

to γ photon detection. For γ-ray detection, electron-hole pairs are generated at each position of the detector, due to the relatively large penetration depth, as shown in Fig.R1 (b), that is, electrons and holes will drift to the electrodes[3] (Zhong He, *Nucl. Instrum. Meth. A* **463**, 250, 2001). Therefore, from the perspective of drift distance, whether detecting α-particles or γ-rays detection, holes need to drift a long distance before reaching the electrode.

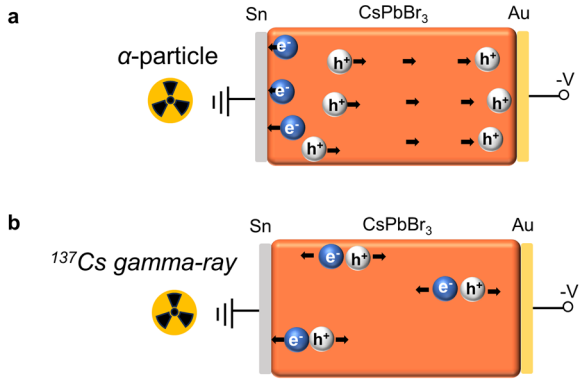

Fig. R1 Schematic diagram of electron and hole drift processes of $CsPbBr_3$ detector. (a) α-particles. (b) γ-rays.

From the perspective of charge collection, Mercouri G. Kanatzidis[1]. adopted a single-hole sensing device that weakens the contribution of electron collection efficiency and improves the efficiency of hole collection. They also point out that the charge collection efficiency of this single-hole device is almost entirely contributed by the hole. Similarly, the charge collection efficiency of α-particle in our manuscript is mainly contributed by the holes, as shown in Fig. R2. Therefore, the total charge collection efficiency of both $CsPbBr_3$ α-particle detectors and gamma-ray detectors depends mainly on the contribution of the hole.

Thus, achieving high energy resolution for the perovskite α-particle detector is challenging both in charge drift and collection.

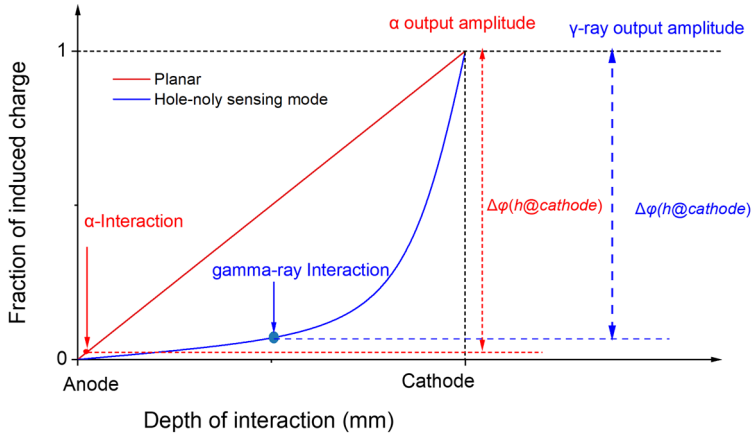

Fig. R2 Schematic diagram of cathode and anode induced charge in planar and hole-only sensing mode.

Question (b): We appreciate the valuable suggestions from the reviewer. To address these concerns, we have conducted comprehensive validation using both theoretical calculation and experimental for detectors of different thicknesses.

Firstly, we simulated the energy resolution of $CsPbBr_3$ detectors with different thicknesses in the air using Geant4, Comsol, and Matlab, as shown in Fig. R3. As the thickness decreases, the energy resolution of the detector improves slightly.

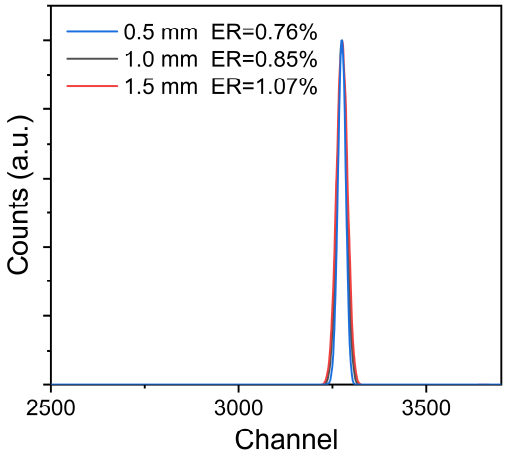

Fig. R3 The theoretical spectra of $CsPbBr_3$ detector with different thicknesses for α-particle.

Secondly, to conduct a detailed analysis of thickness effects, we performed α-particle energy spectrum response experiments using commercial CdZnTe and $CsPbBr_3$ single crystals at varying thicknesses, respectively. The detector size we used initially was 5 mm × 5 mm. However, when thinned down to 0.7 mm by polishing, some crystals experienced slight breaking, resulting in detector sizes smaller than 5 mm × 5 mm at thicknesses of 0.7 mm and 0.5 mm. This phenomenon is more common in large size crystals, such as 10 mm × 10 mm or larger, the crystals frequently suffer broken (Fig. R4).

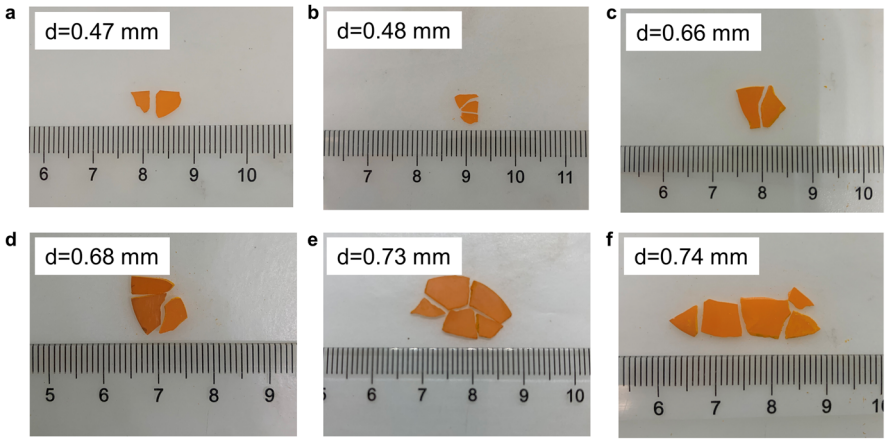

Fig. R4 The broken $CsPbBr_3$ single crystal with different sizes and thicknesses.

By decreasing the thickness, the energy resolution for both the CdZnTe and $CsPbBr_3$ detectors is improved (Figs. R5 and R6). However, when the thickness of $CsPbBr_3$ is further reduced to 500 μm, the improvement in energy resolution is very limited due to the polishing and cutting that introduced defect layers (Fig. R6). We performed multiple sets of replicated experiments with consistent results. As can be seen from Table R1, CdZnTe and $CsPbBr_3$ are typically soft-brittle materials, making them challenging to process. Unlike commercially available CdZnTe detectors with mature surface processing techniques, the polishing processes for $CsPbBr_3$ are still in the exploratory stage. Therefore, $CsPbBr_3$ is more likely to introduce surface structural defects during polishing, which is a key factor hindering further improvement in energy resolution. We will continue to explore and improve the surface treatment technology for perovskite in subsequent studies.

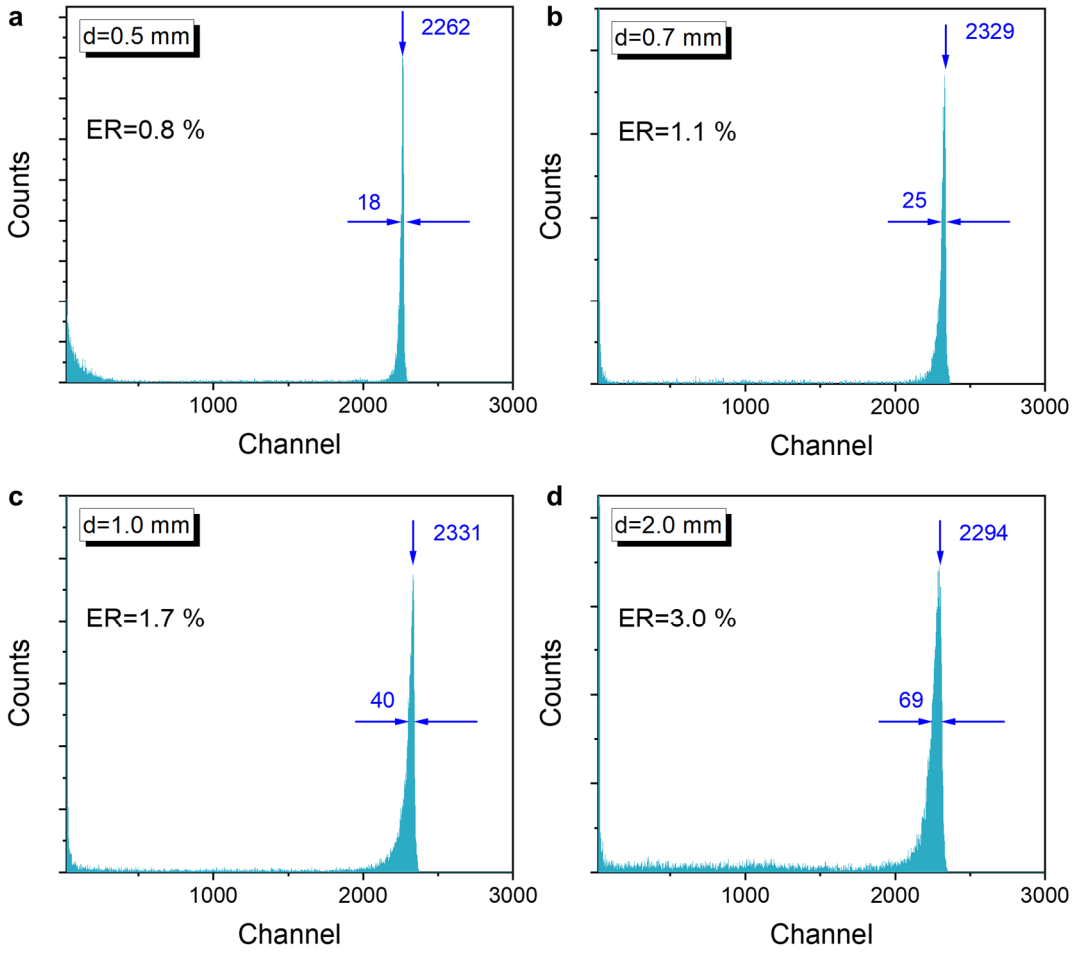

Fig. R5 The spectra of CdZnTe detector with different thicknesses for α-particle (electric field is 1000 $V \cdot cm^{-1}$). (a) 0.5 mm and (b) 0.7 mm (c) 1.0 mm and (d) 2 mm.

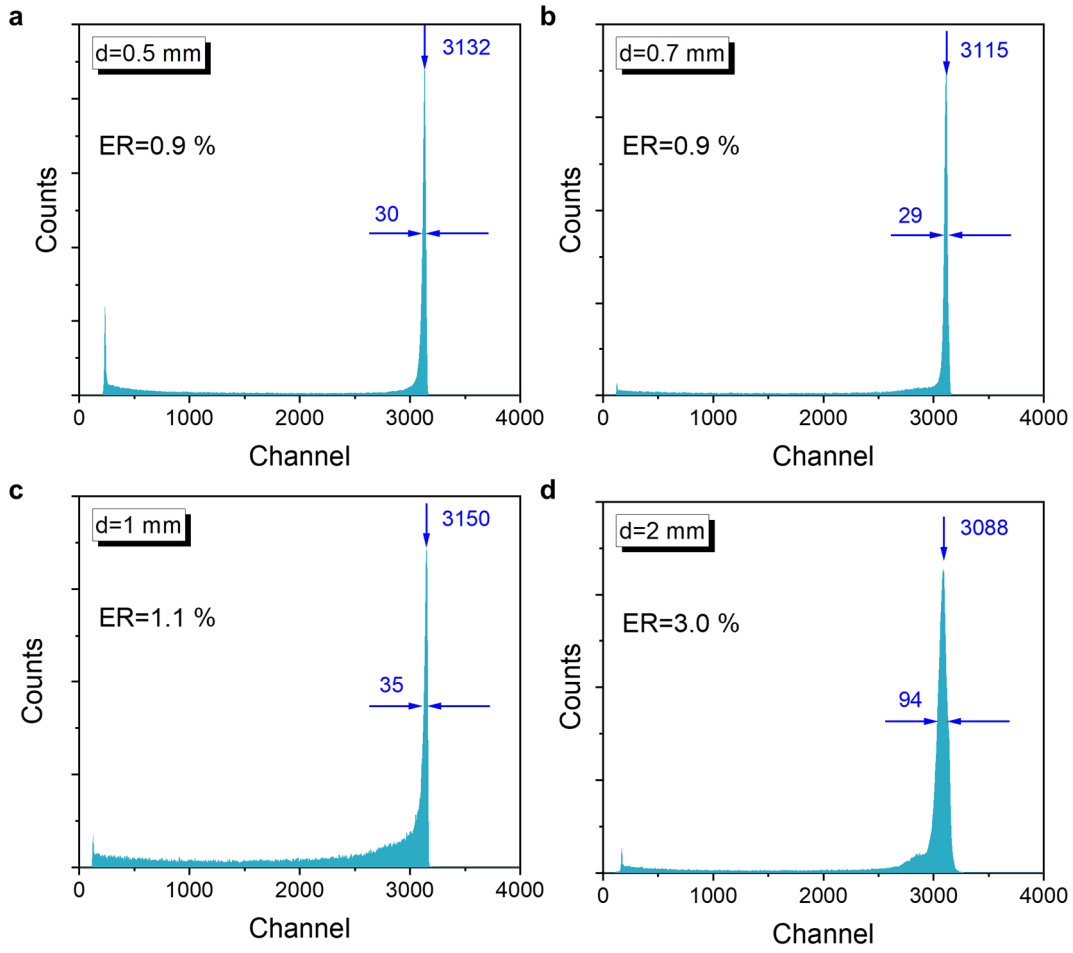

Fig. R6 The spectra of $CsPbBr_3$ detector with different thicknesses for α-particle (electric field is 900 $V \cdot cm^{-1}$). (a) 0.5 mm and (b) 0.7 mm (c) 1.0 mm and (d) 2 mm.

Table R1. Mechanical constants of $CsPbBr_3$ and other materials[4].

Materials	Fracture Toughness ($MPa\ m^{1/2}$)	Hardness (GPa)	Young's modulus (GPa)
CdZnTe[5]	0.146	~0.6	~27
CdTe	0.158	0.76	52
Si	~0.82	12.7	169
$CsPbBr_3$	<0.145[6]	0.34	~15.8

We can fully understand the reviewer's suggestion that using thinner detector can achieve better performance, but there are several points we would like to emphasize considering the practical applications.

- A 700-800 nm perovskite film (polycrystals) is enough to absorb the sunlight and is also suitable for practical applications. However, for the perovskite α-particle and γ-ray detector, achieving a large size single crystal of $CsPbBr_3$ with a thickness on the order of micrometers is challenging. Typically, such crystals need to be cut and polished, which can introduce

surface damage and lead to the enrichment of defect layers, similar to processing methods employed for commercial materials like Si, GaAs, and CdZnTe[7]. **Taking the CdZnTe α-particle detector that has been used commercially as an example, the thickness is usually between 700 um and 1 mm, which can ensure good energy resolution and mechanical properties of the detector**[8, 9]. Therefore, α-particle single-crystal detectors are not always as thin as possible in practice applications.

- On the other hand, if the $(\mu\tau)_h$ value of the $CsPbBr_3$ detector is 10^{-4} $cm^2 \cdot V^{-1}$, the average carrier drift length λ under an electrical field of 2000 $V \cdot cm^{-1}$ is $\lambda=(\mu\tau)_h E$=2 mm, which is much larger than the thickness of the detector. Therefore, **the $CsPbBr_3$ detector with a thickness of 1 mm does not ruin the charge collection efficiency.**

- Furthermore, the developed $CsPbBr_3$ detector is not only suitable for α-particle with energy in the range of a few MeV, but can also be used in the future for detecting protons and heavy charged particles with energy exceeding 10 MeV or even higher. The penetration depth of these particles ranges from tens to hundreds of micrometers. Thus, to ensure the thickness of the sensitivity zone is suitable for high-energy particles, the detector must not be as thin as possible.

Changes in manuscript: Figs. R6a, b, and d are added as Supplementary Fig. 20.

"In Fig. 5e, the designed $CsPbBr_3$ detector obtained the highest ER of 1.1% with a peaking time of 2.5 μs under ambient conditions, rivaling the ER achieved by the CdZnTe detector with the same measurement system (Fig. S19). At the same time, different thicknesses of the $CsPbBr_3$ detector on the spectral response of α particles are shown in Fig.S20. While thinner detectors can achieve an optimal spectral resolution of 0.9%, thinner $CsPbBr_3$ crystals are more prone to breaking due to increased surface enrichment introduced by polishing and cutting. Therefore, to ensure both energy resolution and mechanical properties, the detector thickness is not as thin as possible."

3. The resistivity value is still derived out of the range of working bias...

Response: We thank the reviewer for the classical question.

We re-fit the resistivity under different voltages, as shown in Fig. R7. The resistance is higher than 10^9 Ω·cm at different voltages. When the bias voltage is much smaller, the resistance of the bulk semiconductor limits the leakage current and the bulk resistance can be determined from the fit of the linear *I-V* curve. However, as the voltage increases, the *I-V*

gradually deviates from the linear fit, leading to inaccurate resistivity. At the same time, the R-squre and Pearson's coefficient of linear fitting gradually decreased, indicating that the fitting correlation decreased. Particularly, the leakage current increases rapidly for Au/$CsPbBr_3$/Au devices under a high electric field due to hole injection, as seen in Fig. R8.

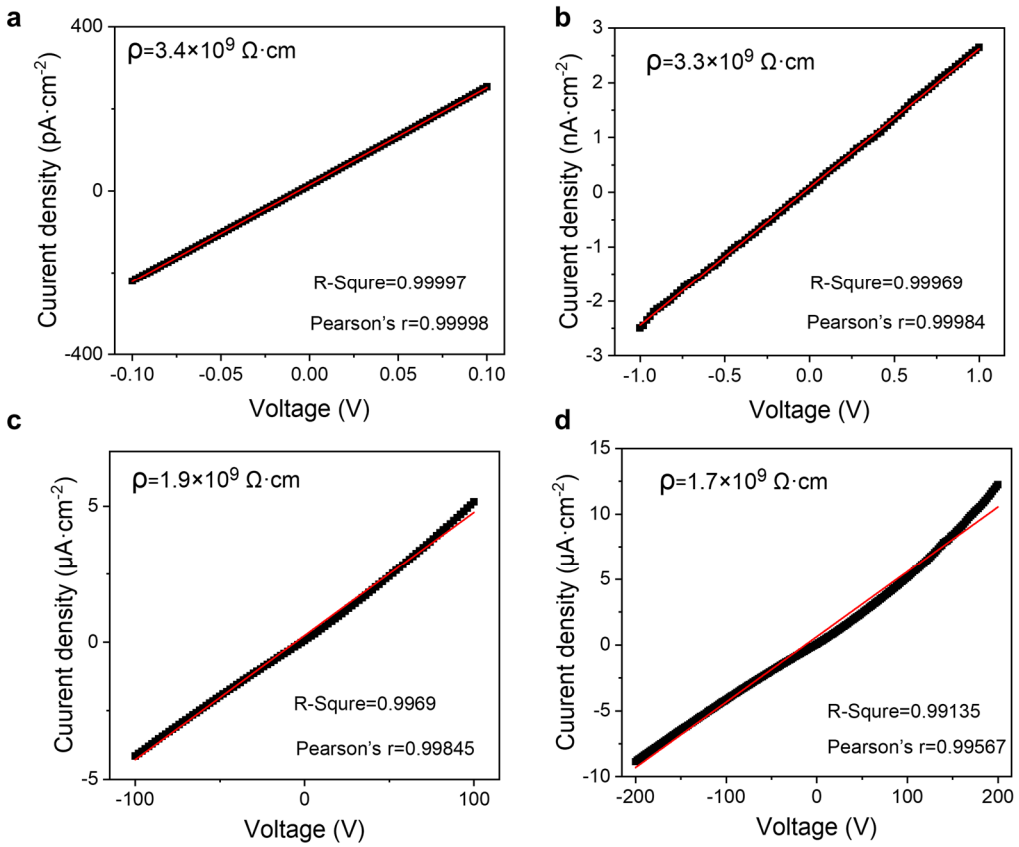

Fig. R7 *I-V* characteristics measured on Au/$CsPbBr_3$/Au device and linear fit in the bulk resistivity ranging from (a) -0.1 V to 0.1 V and (b) -1 V to 1 V (c) -100 V to 100 V and (d) -200 V to 200 V (crystal thickness is 1.2 mm).

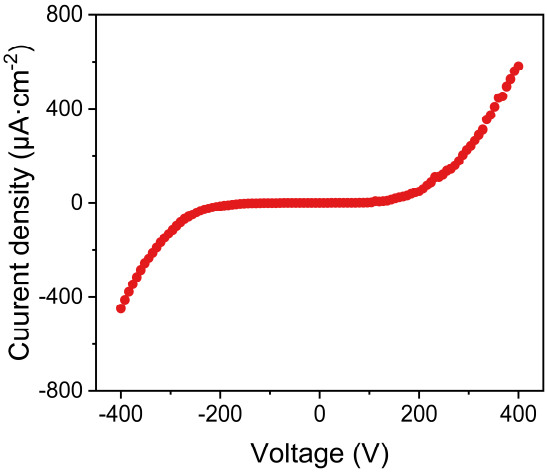

Fig. R8 Current-voltage characteristics in the voltage range -400 V to 400 V measured on Au/$CsPbBr_3$/Au device.

The reference "*J. Appl. Phys*. 100, 014503 (2006)"[10], explained that the accurate measurement of crystal resistivity and surface leakage of semiconductor radiation detectors should be carried out at low bias in detail.

In the measurement of bulk resistivity in high and low resistivity materials, careful preparation of Ohmic contacts is essential for accurate measurements. On one hand, the influence of surface states and contact resistance make it difficult to achieve ideal Ohmic contact between metal and semiconductor. Compared to low voltages where the electric field can evenly distribute in the crystal thickness direction, the electric field concentrates at the metal-semiconductor interface under high voltages, which renders the measurement results unable to correspond to the crystal's bulk resistivity. However, such quasi-Ohmic behavior can be generally obtained if the bias voltage is small enough. There is no significant contribution of the contact barrier on the measured bulk resistance in the low-bias regime (*J. Appl. Phys*. **100**, 014503 2006)[10]. **"When the bias voltage is much smaller than $\pm V_c$, the series resistance of the bulk semiconductor limits the leakage current and the bulk resistance can be determined from the fit of the linear *I-V* curve[10, 11] (Fig. R9)".**

On the other hand, high voltages will involve the crystal surface in conduction, obscuring the information of bulk current and often causing deviations from linearity in *I-V* results (Fig. R10a). Additionally, the leakage current under a high electric field continuously increases over time as extra holes are injected into the system for the $CsPbBr_3$ detector (Fig. R10b, *Nat. Commun*. **9**, 1609, 2018)[12]. Our experimental results are consistent with those reported by the Mercouri G. Kanatzidis group.

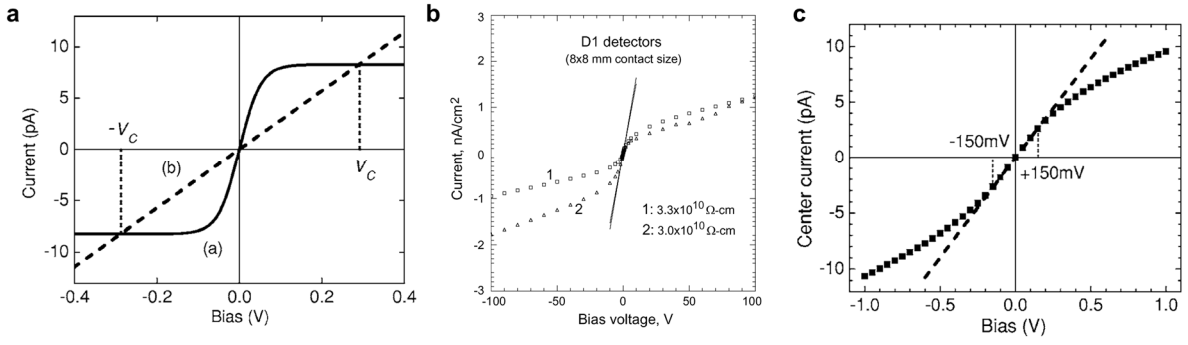

Fig. R9 *I-V* measurement. (a) Ideal thermionic current-voltage characteristics without series resistance and bulk *I-V* curve[10]. (b) *I-V* characteristic measured for two CdZnTe detectors[11].(c) Linear fit in the bulk conductivity limited range[10].

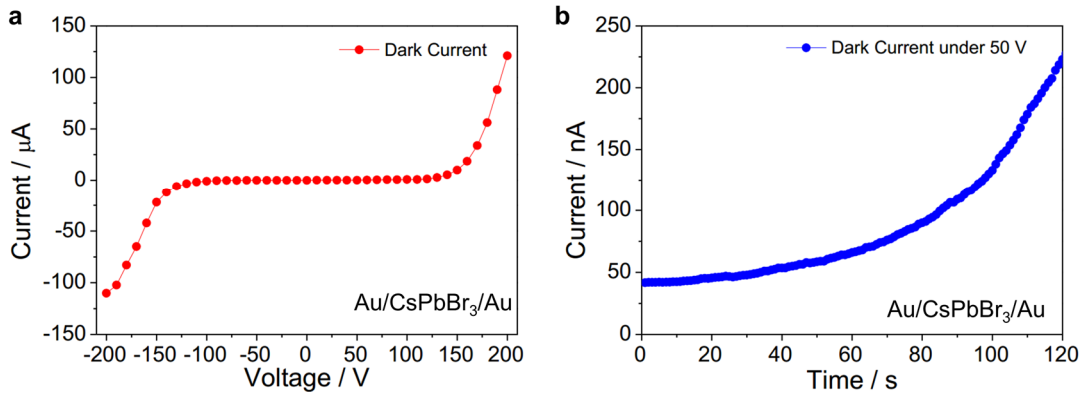

Fig. R10 *I-V* curve in the large bias range of Au/CsPbBr$_3$/Au detector. (d) Dark current variation with time under positive 50 V[12].

In the field of semiconductor detection, the measurement of bulk resistivity has been standardized, that is, using the *I-V* curve at low voltage to fit the resistivity, rather than using the *I-V* curve at operating bias. We can find many references, including bulk resistivity measurements from traditional CdZnTe[10], SiC[13], and perovskites[14-16]. For example, Mercouri G. Kanatzidis[16] revealed the resistivity measurement for $CsPbCl_3$ in the voltage of -1 V to 1 V(*J. Am. Chem. Soc.* 143, 2068, 2021). Shengzhong Liu[17] also reported the resistivity measurement for $MA_3Bi_2I_9$ under the voltage of 0 V to 10 V (*Adv. Opt. Materials* 8, 2000814, 2020), and Jiang Tang[18] calculated the $Cs_2AgBiBr_6$ bulk resistivity at the voltage of -5 V to 5 V (*Nat. Photonics* 11, 726-732, 2017).

Therefore, we believe that the high working bias mentioned by the reviewer refers to the Au/CsPbBr$_3$/Sn devices for spectral testing, which is distinct from the voltage range employed for Au/CsPbBr$_3$/Au devices utilized in resistivity measurements.

Reviewer #3 (Remarks to the Author):

The authors have made good efforts addressing the comments, however, I'm not fully convinced by the discussion for the rise time distribution. It is not obvious from the discussion of why the distribution gets narrower because of the wider band gap. Much more detailed discussion is needed.

Response: We appreciate the Reviewer's recognition and the positive comments. Your valuable suggestions help us to improve the quality of our manuscript. To investigate the temperature dependence of rise time distribution, we conducted multiple sets of experiments involving different voltages, temperatures, and the number of rise time collections. At the same time, we compared the variation of half-peak width with temperature increases.

The output pulse of the $CsPbBr_3$ detector from the charge-sensitive preamplifier possesses various rise times. The inevitable capacitance between the detector and the preamplifier generates noise, leading to variations in rise time distribution[19]. On the other hand, the peak width of the rise time distribution slightly fluctuates with increasing temperature due to statistical fluctuations. To verify that the fluctuation of half peak width is attributed to the influence of statistical fluctuation, we collected the rise time of 1000, 2000, 3000, and 5000 traces in total at a voltage of -100 V, respectively, as shown in Fig. R11. It can be seen that in a small number of statistics, the statistical fluctuation of the distribution of rising time is relatively large, i.e., the distribution of rising time is relatively wide. With the increase in the number of statistics, the fluctuation decreases, which suggests no significant changes for the half-peak width at the temperature range from RT to 343 K. Under the condition of 5000 collections, the half-peak widths from RT to 343 K are 2.59 us, 2.62 us, 2.63 us, and 2.67 us, respectively. Thus, we included that the statistical quantity is critical for accurately measuring rise time distribution.

Generally, we focus on the central value of the rise time distribution (Fig. R12)[20]. As the temperature increases, the variation in the rise time is limited, and the central value of the statistical distribution slightly increases from 3.1 μs at room temperature to 3.4 μs at 343 K (Fig. R11). In the mobility and transit time formula $\mu=\frac{v_{dr}}{E}=\frac{d^2}{Vt_{dr}}$, when the drift time t_{dr} increases with temperature, the mobility decreases. the wider bandgap of our $CsPbBr_3$ detector exhibits a small variation in hole mobility, which offers the capability for higher operating temperatures. It is consistent with the conclusion in classical semiconductor physics (Fig. R13).

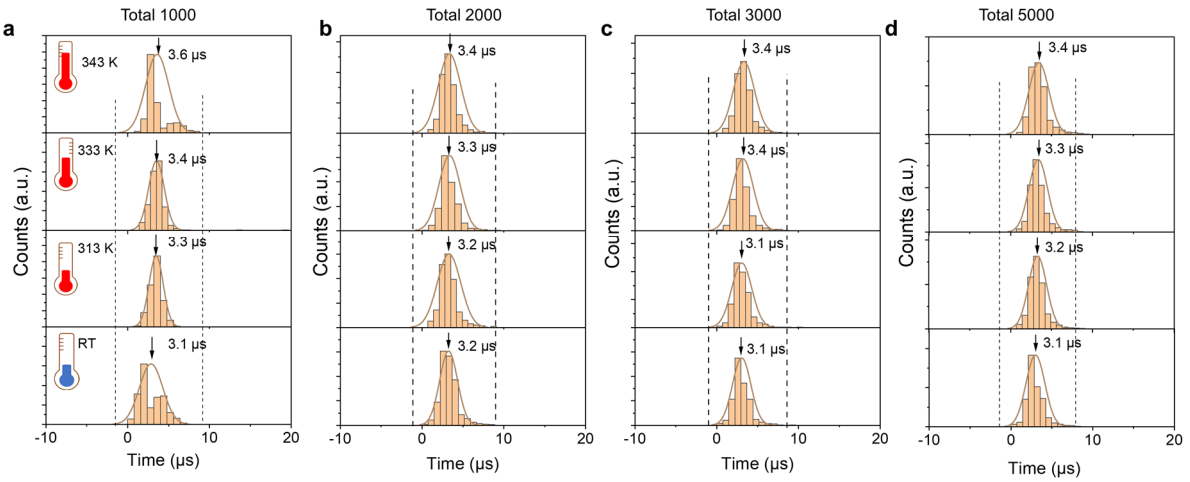

Fig. R11 Statistical distribution of rise time at -100 V. Total traces of (a)1000, (b)2000, (c)3000 and (d)5000.

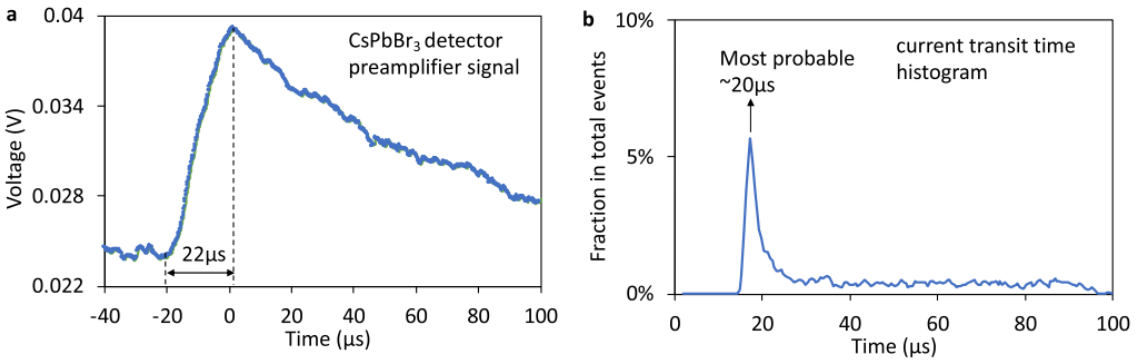

Fig. R12 Voltage pulse and transit times of $CsPbBr_3$ detector. (a) Preamplifier waveform signal. (b) Histogram distribution of rise time[20].

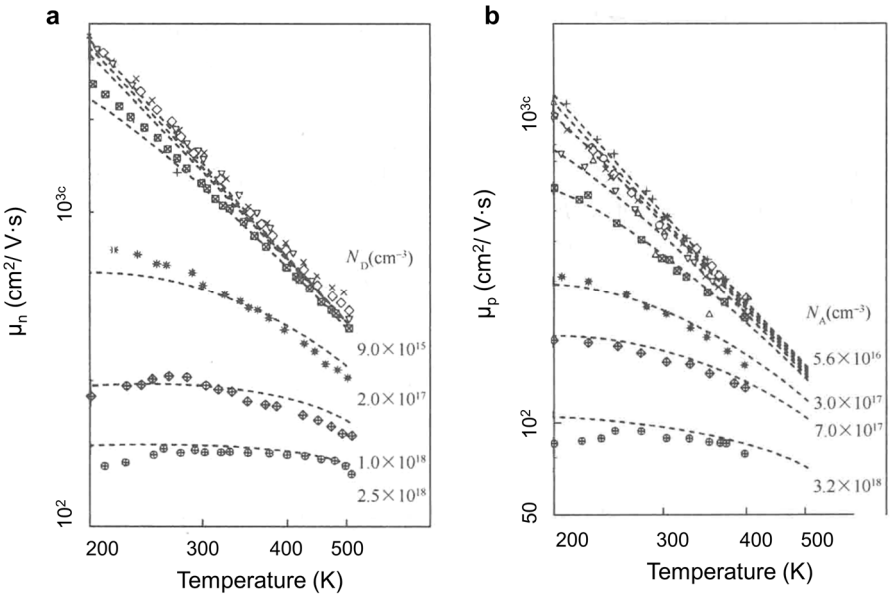

Fig. R13 The electron and hole mobility of Si with increasing temperature. (a) Electron mobility. (b) Hole mobility (The Physics of Semiconductors, Liu Enke, 2017).

We also investigated the rise time distribution under different voltages to further validate the impact of the total number of collections, as shown in Figs. R14 and R15. The rise time statistical distributions at -10 V and -200 V are the same as at -100 V. Therefore, as the number of collections increases, the error caused by statistical fluctuations can be eliminated, and the distribution of rise time does not change.

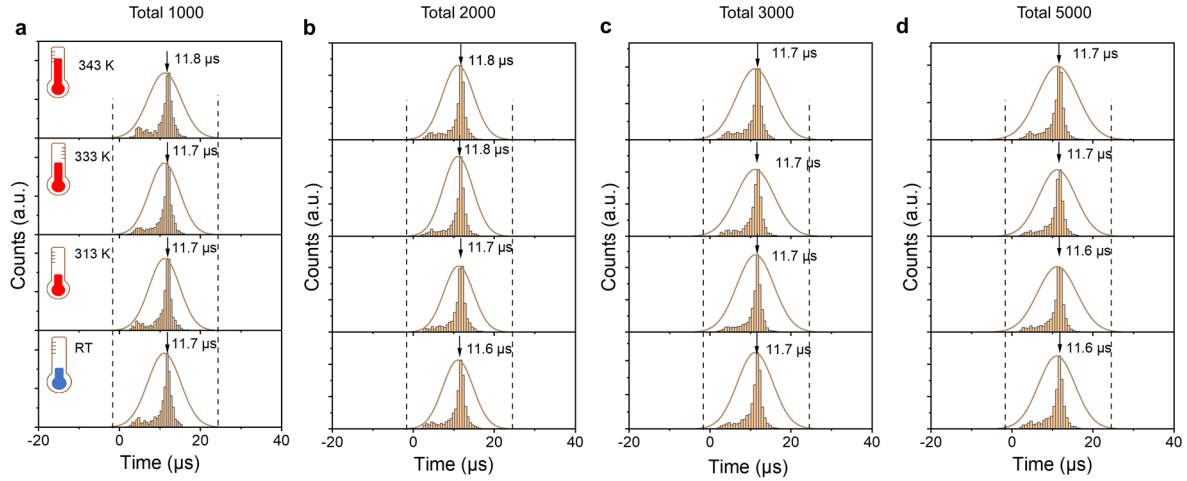

Fig. R14 Statistical distribution of rise time at -10 V. Total traces of (a)1000, (b)2000, (c)3000 and (d)5000.

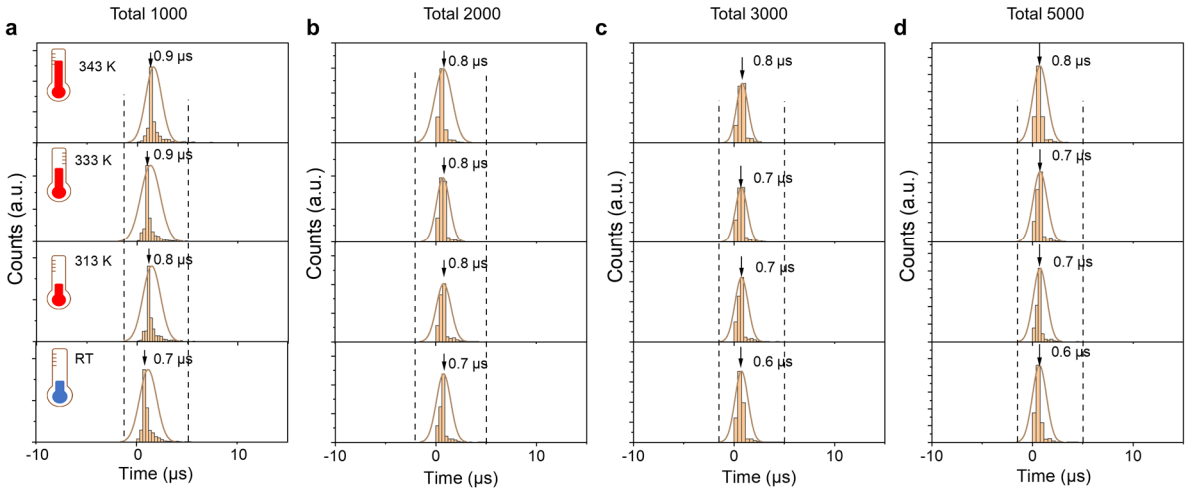

Fig. R15 Statistical distribution of rise time at -200 V. Total traces of (a)1000, (b)2000, (c)3000 and (d)5000.

In conclusion, the distribution of rise time is related to the number of collections, which dominates statistical variations with increasing temperature. At the same time, the rise time is slightly affected by temperature due to the wider bandgap of $CsPbBr_3$ single crystals.

In order to ensure the accuracy of data, 5000 statistical fluctuations of collections were re-distributed in Fig.4a, b, e and Fig. S13, the hole mobility was re-calculated in Fig. 4c. It is important to note that nothing has changed in our conclusions.

Changes in manuscript: Fig.4a-c, and Fig. 4e have been changed. Fig. S13 has also been changed.

"For reliable statistics, a total of 5000 traces were measured for each voltage under air and vacuum, respectively, and the corresponding distribution histograms of the rise time (Figs. 4a and 4b) were used to calculate the hole drift time t_{dr}."

Reference

1. He, Y., et al., $CsPbBr_3$ perovskite detectors with 1.4% energy resolution for high-energy γ-rays. *Nat. Photonics* ***15***, 36-42 (2020).
2. Zhang, M., et al., Metal-semiconductor-metal-nanostructured $CsPbBr_3$ crystal detector for long-term stable α-particle detection. *ACS Appl. Nano Mater.* ***5***, 16039-16044 (2022).
3. He, Z., Review of the Shockley-Ramo theorem and its application in semiconductor gamma-ray detectors. *Nucl. Instrum. Meth. A* ***463***, 250-267 (2001).
4. Rakita, Y., et al., Mechanical properties of $APbX_3$ (A = Cs or CH_3NH_3; X= I or Br) perovskite single crystals. *MRS Communications* ***5***, 623-629 (2015).
5. Li, Y., et al., Nanomechanical behaviors of (110) and (111) CdZnTe crystals investigated by nanoindentation. *Rare Metals* ***28***, 570-575 (2009).
6. Kim, D. B., et al., Anisotropic in situ strain-engineered halide perovskites for high mechanical flexibility. *Adv. Funct. Mater.* ***31***, 2007131 (2020).
7. Zha, G., et al., The study on the surface state of CdZnTe (110) surface. *Appl. Surf. Sci.* ***252***, 8421-8423 (2006).
8. Amman, M., et al., *Alpha particle response characterization of CdZnTe*. SPIE: 2001; Vol. 4507.
9. Povinec, P., et al., Aerosol radioactivity monitoring in Bratislava following the Chernobyl accident. *J. Radioanal. Nucl. Ch.* ***126***, 467-478 (1988).
10. Prokesch, M.; Szeles, C., Accurate measurement of electrical bulk resistivity and surface leakage of CdZnTe radiation detector crystals. *J. Appl. Phys.* ***100***, 014503 (2006).
11. Bolotnikov, A. E., et al., Properties of Pt Schottky type contacts on high-resistivity CdZnTe detectors. *Nucl. Instrum. Meth. A* ***482***, 395-407 (2002).
12. He, Y., et al., High spectral resolution of gamma-rays at room temperature by perovskite $CsPbBr_3$ single crystals. *Nat. Commun.* ***9***, 1609 (2018).
13. Muzykov, P. G., et al., High resistivity measurement of SiC wafers using different techniques. *J. Electron Mater.* ***32***, 505-510 (2003).
14. Zhou, Y., et al., Self-powered perovskite photon-counting detectors. *Nature* ***616***, 712-718 (2023).
15. He, Y., et al., Perovskite $CsPbBr_3$ single crystal detector for alpha-particle spectroscopy. *Nuclear Nucl. Instrum. Meth. A* ***922***, 217-221 (2019).
16. He, Y., et al., Demonstration of energy-resolved γ-ray detection at room temperature by the $CsPbCl_3$ perovskite semiconductor. *J. Am. Chem. Soc.* ***143***, 2068-2077 (2021).
17. Liu, Y., et al., Large Lead-free perovskite single crystal for high-performance coplanar x-ray imaging applications. *Adv. Opt. Mater.* ***8***, 2000814 (2020).
18. Pan, W., et al., $Cs_2AgBiBr_6$ single-crystal X-ray detectors with a low detection limit. *Nat. Photonics* ***11***, 726-732 (2017).
19. Amrami, R., et al., Timing performance of pixelated CdZnTe detectors. *Nucl. Instrum. Meth. A* ***458***, 772-781 (2001).
20. Pan, L., et al., Performance of perovskite $CsPbBr_3$ single crystal detector for gamma-ray detection. *IEEE T. Nucl. Sci.* ***67***, 443-449 (2020).

REVIEWERS' COMMENTS

Reviewer #2 (Remarks to the Author):

I have no further concerns.

Reviewer #3 (Remarks to the Author):

The authors have addressed my concern. I don't have further comments and support its publication.